



GJK++: Leveraging Acceleration Methods for Faster Collision Detection

Louis Montaut, Quentin Le Lidec, Vladimír Petrík, Josef Sivic, Justin Carpentier

► To cite this version:

Louis Montaut, Quentin Le Lidec, Vladimír Petrík, Josef Sivic, Justin Carpentier. GJK++: Leveraging Acceleration Methods for Faster Collision Detection. IEEE Transactions on Robotics, In press, 10.1109/TRO.2024.3386370 . hal-04070039v3

HAL Id: hal-04070039

<https://hal.science/hal-04070039v3>

Submitted on 3 Apr 2024

HAL is a multi-disciplinary open access archive for the deposit and dissemination of scientific research documents, whether they are published or not. The documents may come from teaching and research institutions in France or abroad, or from public or private research centers.

L'archive ouverte pluridisciplinaire **HAL**, est destinée au dépôt et à la diffusion de documents scientifiques de niveau recherche, publiés ou non, émanant des établissements d'enseignement et de recherche français ou étrangers, des laboratoires publics ou privés.



Distributed under a Creative Commons Attribution - NoDerivatives 4.0 International License

GJK++: Leveraging Acceleration Methods for Faster Collision Detection

Louis Montaut, Quentin Le Lidec, Vladimir Petrik, Josef Sivic and Justin Carpentier, *Member, IEEE*

Abstract—Collision detection is a fundamental problem in various domains, such as robotics, computational physics, and computer graphics. In general, collision detection is tackled as a computational geometry problem, with the so-called Gilbert, Johnson, and Keerthi (GJK) algorithm being the most adopted solution nowadays. While introduced in 1988, GJK remains the most effective solution to compute the distance or the collision between two 3D convex geometries. Over the years, it was shown to be efficient, scalable, and generic, operating on a broad class of convex shapes, ranging from simple primitives (sphere, ellipsoid, box, cone, capsule, etc.) to complex meshes involving thousands of vertices. In this article, we introduce several contributions to accelerate collision detection and distance computation between convex geometries by leveraging the fact that these two problems are fundamentally optimization problems. Notably, we establish that the GJK algorithm is a specific sub-case of the well-established Frank-Wolfe (FW) algorithm in convex optimization. By adapting recent works linking Polyak and Nesterov accelerations to Frank-Wolfe methods, we also propose two accelerated extensions of the classic GJK algorithm. Through an extensive benchmark over millions of collision pairs involving objects of daily life, we show that these two accelerated GJK extensions significantly reduce the overall computational burden of collision detection, leading to computation times that are up to two times faster. Finally, we hope this work will significantly reduce the computational cost of modern robotic simulators, allowing the speed-up of modern robotic applications that heavily rely on simulation, such as reinforcement learning or trajectory optimization.

Index Terms—Convex Optimization, Collision Detection, Computational Geometry, Computer Graphics, Simulation, Trajectory Optimization, Motion Planning

I. INTRODUCTION

PHYSICS engines designed to simulate rigid bodies are an essential tool used in a wide variety of applications, notably in robotics, video games, and computer graphics [1]–[3]. Collision detection, a crucial feature of any physics engine or robot motion planner [4]–[6], consists of finding which objects are colliding or not, *i.e.* are sharing at least one common point or if there exists a separating hyper-plane between both. As simulation often needs to deal with multiple objects and run in real-time (*i.e.*, in video games) or at very high frequencies (*i.e.*, in robotics), collision detection must be carried out as fast as possible. To reduce computational times, collision detection is

Louis Montaut, Vladimir Petrik and Josef Sivic are with the Czech Institute of Informatics, Robotics and Cybernetics, Czech Technical University in Prague.

Louis Montaut, Quentin Le Lidec and Justin Carpentier are with Inria and Département d'Informatique de l'École Normale Supérieure, PSL Research University in Paris, France.

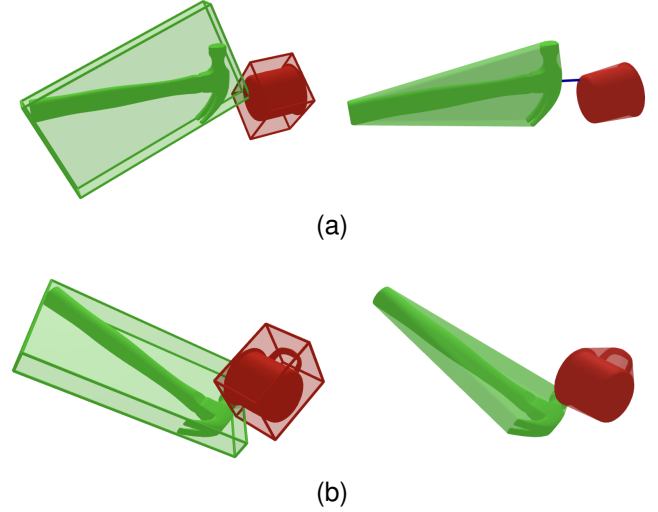


Fig. 1. Two distinct collision problems using shapes from the YCB dataset: in (a) the shapes \mathcal{A}_1 (in green) and \mathcal{A}_2 (in red) are not in collision ($\text{dist}(\mathcal{A}_1, \mathcal{A}_2) > 0$) whereas in (b) the shapes are in collision ($\text{dist}(\mathcal{A}_1, \mathcal{A}_2) = 0$). In the left column, the oriented bounding boxes (OBB) of the objects are represented in light colors. In the right column, the light colors represent the convex hull of each object. In both collision problems, (a) and (b), the broad phase finds a collision between the object's OBBs; the narrow phase must thus be called to confirm or infirm the collision. The right column corresponds to the narrow phase in which the GJK algorithm is called on the objects' convex hulls. In this paper, we propose the Polyak-accelerated GJK and Nesterov-accelerated GJK algorithms in order to accelerate collision detection.

usually decomposed into two phases thoroughly covered in [7]. The first phase is the so-called *broad phase* which consists in identifying which pair of simulated objects are potentially colliding. The broad phase relies on the simulated objects' bounding volumes, as shown in Fig. 1, allowing to quickly assess if the objects are *not* in collision. The second phase is the so-called *narrow phase* in which each pair identified in the broad phase is tested to check whether a collision is truly occurring. Collision detection during the narrow phase is the focus of this paper.

Problem formulation. We consider two convex shapes \mathcal{A}_1 and \mathcal{A}_2 in \mathbb{R}^n (with $n = 2$ or 3 in common applications). If the shapes are not convex, we use their respective convex hulls or decompose them into a collection of convex sub-shapes [8]. The *separation distance* between \mathcal{A}_1 and \mathcal{A}_2 , denoted by $\text{dist}(\mathcal{A}_1, \mathcal{A}_2) \in \mathbb{R}_+$, can be formulated as a minimization problem of the form:

$$d_{1,2} = \min_{\mathbf{x}_1 \in \mathcal{A}_1, \mathbf{x}_2 \in \mathcal{A}_2} \|\mathbf{x}_1 - \mathbf{x}_2\|^2 \quad (1)$$

and $\text{dist}(\mathcal{A}_1, \mathcal{A}_2) = \sqrt{d_{1,2}}$,

where $x_1 \in \mathcal{A}_1$ and $x_2 \in \mathcal{A}_2$ are both vectors in \mathbb{R}^n , $d_{1,2}$ is the optimal value of (1) and $\|\cdot\|$ is the Euclidian norm of \mathbb{R}^n . If \mathcal{A}_1 and \mathcal{A}_2 intersect (*i.e.*, they are in collision), we necessarily have $\text{dist}(\mathcal{A}_1, \mathcal{A}_2) = 0$. If the two shapes do not intersect, we have $\text{dist}(\mathcal{A}_1, \mathcal{A}_2) > 0$. These two cases are illustrated in Fig. 1.

Problem (1) allows us to consider both the *distance computation* problem and the computationally cheaper *Boolean collision check* as one single convex optimization problem. In the distance computation problem, we aim at computing the separation distance between \mathcal{A}_1 and \mathcal{A}_2 , denoted $\text{dist}(\mathcal{A}_1, \mathcal{A}_2)$, *i.e.* the distance between their closest points. This distance is helpful in some applications such as collision-free path planning [9], [10], especially for pairs of objects entering the narrow phase. If the broad phase has not selected a pair of objects, a cheap estimate of $\text{dist}(\mathcal{A}_1, \mathcal{A}_2)$ is usually enough [7]. In the Boolean collision check, we only aim at determining if \mathcal{A}_1 and \mathcal{A}_2 intersect, and computing $\text{dist}(\mathcal{A}_1, \mathcal{A}_2)$ is unnecessary. However, we will later see that the Boolean collision check is a sub-problem of the distance computation problem: solving (1) can be early-stopped once a separating plane between \mathcal{A}_1 and \mathcal{A}_2 has been found. In the rest of this paper, we will use the generic term “collision detection” to refer to distance computation and Boolean collision checking altogether. We will specify when the distinction is needed.

Contributions and paper outline. Our work builds on the seminal works by [11] and [12] as well as on the work of [13], [14] to globally accelerate distance computation and collision checking algorithms between convex shapes. We make the following contributions:

- In Sec. II, we provide an in-depth tutorial on the state-of-the-art Gilbert-Johnson-Keerthi (GJK) algorithm used to solve collision detection problems. Although it is often presented and discussed as a computational geometry algorithm, we show that GJK is, in fact, a sub-case of the much older fully-corrective Frank-Wolfe (FW) algorithm;
- In Sec. III, we adapt recent works on Polyak and Nesterov-accelerated FW to accelerate both the distance computation and the Boolean collision check problems;
- In Sec. IV, we empirically analyze the convergence of our proposed approach on two large shape benchmarks. Results show a faster convergence of our approach leading to a computational time up to two times faster than the state-of-the-art GJK algorithm on both distance computation and Boolean collision checking. We also provide a benchmark against other collision detection algorithms from the libCCD [15], FCL [16] and BulletCollision [17] collision detection libraries which are used in physics simulators like Drake [18], MuJoCo [3], ODE [19] and Bullet [1].
- We empirically show that GJK-like algorithms, which our proposed methods belong to, are superior by orders of magnitude to generic quadratic programming solvers on collision detection problems;
- Finally, we show that our methods can be used in any physics simulator by benchmarking them on trajectories generated by the Bullet simulator. Like GJK, our methods

can benefit from being warm-started using the previous simulation time steps, enabling temporal coherence for our proposed accelerated collision detection algorithms.

This article is an extended version of a previously published paper [20] which presented the Nesterov-accelerated GJK algorithm. To expand on our previous work, we introduce the Polyak-accelerated GJK algorithm, provide additional benchmarks, notably against existing collision detection libraries, and show that our proposed methods can be used in the context of physics simulation by benefiting from being warm-started using previous simulation steps.

In the rest of this section, we first formulate the problem of collision detection and then provide an overview of collision detection related works.

Related work. The so-called Gilbert-Johnson-Keerthi algorithm (GJK) [12] is the most well-known algorithm for collision detection between two convex shapes. It can handle the distance computation and the Boolean collision check [21]. The expanding polytope algorithm (EPA) [22], an extension to GJK, can compute the penetration depth *i.e.* the norm of the separation vector, when shapes are in collision. The separation vector is the vector of smallest norm needed to translate one of the two shapes such that the two shapes do not intersect. The EPA solves a non-convex and more complex problem than (1), which is not the focus of this paper.

Most alternatives to GJK in the literature focus on computing collisions between convex polyhedra, such as the Lin-Canny algorithm [23] or the V-Clip [24] algorithm. Although GJK is equivalent in performance to these algorithms [25], it is not restricted to convex polyhedra. The strength of GJK is formulating the collision detection problem on the Minkowski difference. The properties of the Minkowski difference are used to cleverly compute support vectors on the Minkowski difference (these notions are introduced and detailed in Sec. II). GJK can thus handle collision detection, and distance computation for many different shapes such as convex polyhedra and basic primitives (*i.e.*, spheres, ellipsoids, cylinders, capsules etc.) [7], [21], [26]. The Minkowski Portal Refinement (MPR) [27] is a variant of the GJK algorithm which is slightly simpler to implement; however, MPR can only perform boolean collision checks as it cannot be used to perform distance computation between non-overlapping shapes. Overall, the generality of GJK, efficiency, good precision, and ease of implementation make it the state-of-the-art algorithm for collision detection between two convex shapes.

Collision detection has been casted into a convex optimization problem for many years [12], [28], [29]. However, collision detection is traditionally presented and considered mainly as a computational geometry problem [7], [21], [24], [25], [30], [31]. Over the years, this computational geometric perspective allowed enhancing the computational efficiency of GJK, thanks to improvements to its internal sub-routines [21], [30]. However, we argue that this view has also limited collision detection improvement. Instead, we propose to tackle collision from the perspective of convex optimization. This correlates with some observations raised in the original GJK papers. Indeed, as briefly mentioned already in their 1988

paper [12] and brought up again by [29], [32], the ideas developed by Gilbert, Johnson, and Keerthi are rooted in convex optimization, notably in the works of [33] and [34] for solving Minimum-Norm Point (MNP) problems. This article proposes exploiting the Frank-Wolfe convex optimization setting to tackle collision detection. In particular, by leveraging recent progresses in acceleration methods in convex optimization [35], we show how to accelerate collision detection by directly lowering the number of iterations needed to solve a collision problem instance compared to the vanilla GJK algorithm.

The Frank-Wolfe algorithm (FW) dates back to 1956 and is one of the first convex optimization algorithms. It has been heavily studied over the years by the optimization community. This algorithm iterates over the computation of *support points* to approach the optimal solution. The undesired zig-zagging behavior of FW, already identified by its authors, has been addressed by introducing corrections to the original FW method [33], [34], [36]–[40]. In [38] and [40], widely used corrections of the FW algorithm are analyzed, and their convergence properties.

In this work, we notably show in Sec. II that the GJK algorithm is an instance of the *fully-corrective* Frank-Wolfe algorithm, covered in [40], applied to solving a MNP problem. Finally, recent works have also tried accelerating the FW algorithm by applying the so-called Nesterov acceleration [41], a classic acceleration technique in unconstrained optimization. Nesterov momentum has been successfully added by [14] to accelerate FW.

II. COLLISION DETECTION FROM A FRANK-WOLFE PERSPECTIVE

In this section, we highlight the natural connection between computing the distance between convex shapes and convex optimization, particularly within the frame of the Frank-Wolfe (FW) setting. The first part of this section is a tutorial on collision detection, starting with FW and gradually working towards GJK. We then show that the GJK algorithm can be seen as a variant of the FW algorithm that leverages properties of convex 3D shapes to lower the computational complexity drastically.

Distance computation and Boolean collision checking. As recalled in Sec. I, collision detection is a sub-case of distance computation: $\text{dist}(\mathcal{A}_1, \mathcal{A}_2) > 0$ means that the two shapes do not overlap while $\text{dist}(\mathcal{A}_1, \mathcal{A}_2) = 0$ means that the shapes are in collision. In the case of $\text{dist}(\mathcal{A}_1, \mathcal{A}_2) > 0$, finding a strictly positive lower bound on $d_{1,2}$ to solve the collision problem is sufficient. In the context of convex shapes, this is often simpler than computing the distance between the two shapes [10] and can be done by finding a plane separating \mathcal{A}_1 from \mathcal{A}_2 . In the rest of the paper, we focus on the generic problem of computing the distance between \mathcal{A}_1 and \mathcal{A}_2 , as it encapsulates the more straightforward Boolean collision check covered later in this section. Results for the particular Boolean collision checking case are analyzed in the

experimental section IV.

Collision detection from the perspective of quadratic programming. From the perspective of numerical optimization, the first idea is to look at problem (1) through the lens of quadratic programming. In the case of meshes, which are shapes represented by soups of 3D points and which faces represented as triangles, we can use the implicit description of a convex mesh as a linear inequality of the form $Ax \leq b$. The collision detection problem between two meshes can thus be cast as a quadratic programming (QP) problem:

$$\begin{aligned} d_{1,2} = \min_{x_1, x_2 \in \mathbb{R}^3} \quad & \|x_1 - x_2\|^2 \\ \text{s.t.} \quad & A_1 x_1 \leq b_1 \\ & A_2 x_2 \leq b_2. \end{aligned} \quad (2)$$

While many off-the-shelf solvers exist to solve QP problems, their performances scale poorly with respect to the number of constraints [42]. This is especially true in the presence of complex meshes composed of hundreds or thousands of vertices, for which QP solvers can take a few milliseconds to assess a collision, as we experimentally highlight in Sec. IV-C. Having established that solving collision detection requires dedicated methods, we turn our attention to solutions such as GJK, which has been shown to operate on a large class of shapes, ranging from simple primitives to very complex meshes.

Recasting the distance computation problem onto the Minkowski difference. The first important idea of 1988's paper by Gilbert, Johnson, and Keerthi [12] is to recast the distance computation problem onto the Minkowski difference \mathcal{D} of the shapes and defined as follows:

$$\mathcal{D} = \mathcal{A}_1 - \mathcal{A}_2 = \{x = x_1 - x_2 \mid x_1 \in \mathcal{A}_1, x_2 \in \mathcal{A}_2\} \subset \mathcal{C}, \quad (3)$$

where $\mathcal{C} = \mathbb{R}^n$ is the so-called *collision space*. The shapes \mathcal{A}_1 and \mathcal{A}_2 lie in the shape space and the Minkowski difference \mathcal{D} lies in the collision space.

Although both the shape space and the collision space are isomorphic to \mathbb{R}^n , we distinguish between the two to highlight the change in perspective. In Fig. 2, we illustrate the link between a pair of two convex shapes and their corresponding Minkowski difference. We stress that the Minkowski difference \mathcal{D} is *specific* to shapes \mathcal{A}_1 and \mathcal{A}_2 . If the relative position or relative orientation between \mathcal{A}_1 and \mathcal{A}_2 changes, their Minkowski difference changes accordingly.

The following properties, illustrated in Fig. 2, hold for the Minkowski difference \mathcal{D} :

- 1) Since \mathcal{A}_1 and \mathcal{A}_2 are convex sets, \mathcal{D} is also convex.
- 2) If \mathcal{A}_1 and \mathcal{A}_2 are intersecting, the origin of \mathcal{C} , denoted as $\mathbf{0}_C$, lies inside the Minkowski difference \mathcal{D} , i.e. $\mathbf{0}_C = x_1 - x_2$ for some $x_1 \in \mathcal{A}_1$ and $x_2 \in \mathcal{A}_2$.
- 3) If \mathcal{A}_1 and \mathcal{A}_2 are not intersecting, the projection of $\mathbf{0}_C$ onto \mathcal{D} , $x^* = \text{proj}_{\mathcal{D}}(\mathbf{0}_C)$, corresponds to two vectors $x_1^* \in \mathcal{A}_1$ and $x_2^* \in \mathcal{A}_2$, also called witness vectors in the computational geometry literature [7]. Contrary to x^* , these vectors x_1^* and x_2^* are not necessarily unique, as

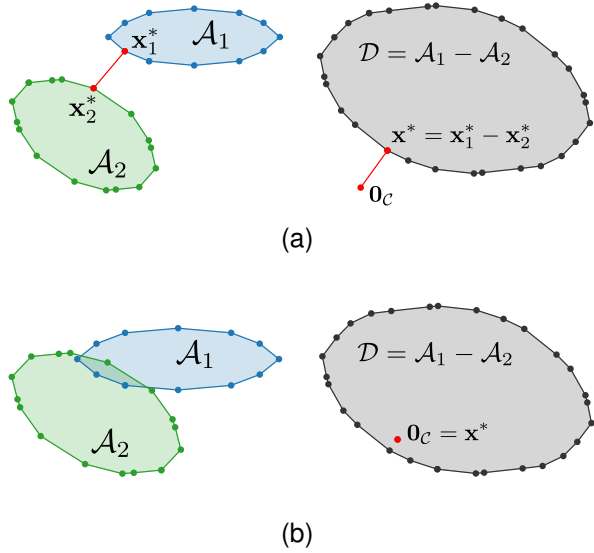


Fig. 2. (a) Distant vs. (b) overlapping pairs of shapes and their respective Minkowski difference. Left column: two convex shapes in 2D. Right column: the Minkowski difference \mathcal{D} of \mathcal{A}_1 and \mathcal{A}_2 . Since \mathcal{A}_1 and \mathcal{A}_2 are convex, \mathcal{D} is also convex. In (a), the shapes are not in collision hence the origin of the configuration space \mathcal{C} , $\mathbf{0}_C$ (in red) lies outside the Minkowski difference, $\mathbf{0}_C \notin \mathcal{D}$. The vector $\mathbf{x}^* = \mathbf{x}_1^* - \mathbf{x}_2^*$ separates \mathcal{A}_1 from \mathcal{A}_2 . It is also equal to the projection of $\mathbf{0}_C$ onto the Minkowski difference \mathcal{D} , $\mathbf{x}^* = \text{proj}_{\mathcal{D}}(\mathbf{0}_C)$. In (b), the shapes overlap, thus $\mathbf{0}_C \in \mathcal{D}$. In this case, we have $\mathbf{x}^* = \text{proj}_{\mathcal{D}}(\mathbf{0}_C) = \mathbf{0}_C$.

is the case for non-strictly convex shapes such as two parallel boxes.

4) Finally, we always have $\|\mathbf{x}^*\| = \text{dist}(\mathcal{A}_1, \mathcal{A}_2)$.

This final remark allows us to recast the distance computation problem (1) onto the Minkowski difference as follows:

$$d_{1,2} = \min_{\mathbf{x} \in \mathcal{D}} \|\mathbf{x} - \mathbf{0}_C\| = \min_{\mathbf{x} \in \mathcal{D}} \|\mathbf{x}\|. \quad (4)$$

The convex optimization problem (4) is equivalent to (1) and is known as a Minimum-Norm Point problem in the optimization literature [34], [40], [43]. In our case, $\mathbf{0}_C \in \mathcal{C} = \mathbb{R}^n$ is the null vector *i.e.* the origin of the collision space. We thus aim at finding the point in \mathcal{D} with the lowest norm. This vector \mathbf{x}^* is the *optimal solution* to (4), given by $d_{1,2} = \|\mathbf{x}^*\| = \text{dist}(\mathcal{A}_1, \mathcal{A}_2)$.

Directly computing the Minkowski difference \mathcal{D} is neither analytically tractable nor computationally efficient. Most of the first and second-order methods for constrained convex optimization problems, such as projected gradient descent or interior point methods [44], are thus sub-optimal choices. However, computing support vectors of the Minkowski difference \mathcal{D} , a notion defined hereinafter in this section, is relatively simple and largely demonstrated by [12]. As we discuss next, solving convex optimization problems by computing support vectors is the strength of the Frank-Wolfe algorithm and its variants [38].

Distance computation using the Frank-Wolfe algorithm.

The Frank-Wolfe algorithm (FW) [11] is one of the oldest convex optimization methods and solves the following constrained optimization problem:

$$f(\mathbf{x}^*) = \min_{\mathbf{x} \in \mathcal{D}} f(\mathbf{x}), \quad (5)$$

Algorithm 1 Frank-Wolfe algorithm with linesearch [38]

Let $\mathbf{x}_0 \in \mathcal{D}$, $\epsilon > 0$

For $k=0, 1, \dots$ **do**

- 1: $\mathbf{d}_k = \nabla f(\mathbf{x}_k)$ ▷ Direction of support
 - 2: $\mathbf{s}_k \in \arg \min_{\mathbf{s} \in \mathcal{D}} \langle \mathbf{d}_k, \mathbf{s} \rangle (= S_{\mathcal{D}}(\mathbf{d}_k))$ ▷ Support (8)
 - 3: **If** $g_{FW}(\mathbf{x}_k) \leq \epsilon$, **return** $f(\mathbf{x}_k)$ ▷ Duality gap (16)
 - 4: $\gamma_k = \arg \min_{\gamma \in [0,1]} f(\gamma \mathbf{x}_k + (1-\gamma)\mathbf{s}_k)$ ▷ Linesearch
 - 5: $\mathbf{x}_{k+1} = \gamma_k \mathbf{x}_k + (1-\gamma_k)\mathbf{s}_k$ ▷ Update iterate
- In the case of the distance computation problem (4), where $f(\mathbf{x}) = \|\mathbf{x}\|^2$, line 4-5 correspond to projecting $\mathbf{0}_C$ on the segment $[\mathbf{x}_k, \mathbf{s}_k]$:*
- 6: $\mathbf{x}_{k+1} = \text{proj}_{[\mathbf{x}_k, \mathbf{s}_k]}(\mathbf{0}_C)$ ▷ Project $\mathbf{0}_C$ on $[\mathbf{x}_k, \mathbf{s}_k]$

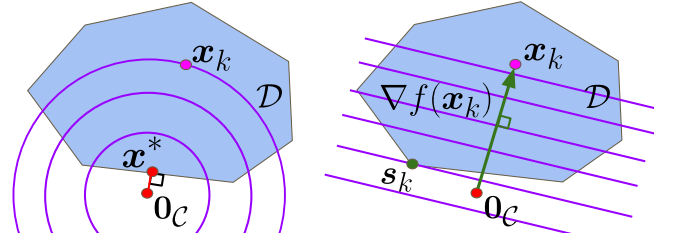


Fig. 3. Computing a support vector \mathbf{s}_k in direction $\nabla f(\mathbf{x}_k)$ on convex set \mathcal{D} . We illustrate with the example of distance computation. On the left, we draw the Minkowski difference \mathcal{D} of which point of minimum norm (MNP) is \mathbf{x}^* *i.e.* \mathbf{x}^* is the projection of $\mathbf{0}_C$ onto \mathcal{D} , $\mathbf{x}^* = \text{proj}_{\mathcal{D}}(\mathbf{0}_C)$. The iterate at iteration k of the FW algorithm is \mathbf{x}_k . In purple we draw the level sets of the function $f(\mathbf{x}) = \|\mathbf{x}\|^2$. On the right, we draw in purple the level sets of the linearization of f at iterate \mathbf{x}_k , h_k . The first step of the FW algorithm is to compute support vector \mathbf{s}_k in the direction of $\nabla f(\mathbf{x}_k)$ (green arrow), $\mathbf{s}_k \in S_{\mathcal{D}}(\nabla f(\mathbf{x}_k))$. In the second step of the FW algorithm, we compute \mathbf{x}_{k+1} as a convex combination of \mathbf{x}_k and \mathbf{s}_k *i.e.* \mathbf{x}_{k+1} is a point on the segment $[\mathbf{x}_k, \mathbf{s}_k]$.

where $f: \mathbb{R}^n \rightarrow \mathbb{R}$ is a convex and differentiable function and \mathcal{D} is a compact convex set. For our distance computation problem (4), we use $f(\mathbf{x}) = \|\mathbf{x}\|^2$ and the Minkowski difference \mathcal{D} as convex constraint set. As a side note, the following discussed algorithms all require an initial starting point $\mathbf{x}_0 \in \mathcal{D}$. Shapes used in physics engines are usually attached to a frame to keep track of their position and orientation in space. We denote $\mathbf{c}^1 \in \mathcal{A}_1$ and $\mathbf{c}^2 \in \mathcal{A}_2$ the origins of the frames attached to \mathcal{A}_1 and \mathcal{A}_2 , respectively. In the rest of this paper, we take $\mathbf{x}_0 = \mathbf{c}^1 - \mathbf{c}^2$.

The FW algorithm, summarized in Alg. 1, is a gradient-descent method. It consists in iteratively applying two steps in order to converge towards the optimal solution \mathbf{x}^* of (5). If we denote by \mathbf{x}_k the estimate of \mathbf{x}^* at iteration k , these two steps correspond to:

- 1) First, we compute a support vector \mathbf{s}_k in the direction of $\nabla f(\mathbf{x}_k)$, by solving a linear optimization problem on \mathcal{D} .
- 2) Second, we update our current iterate \mathbf{x}_k to obtain \mathbf{x}_{k+1} , by taking a convex combination of the current iterate \mathbf{x}_k and the computed support vector \mathbf{s}_k .

In the following, we detail these steps in the context of distance computation. At iteration k , the current iterate \mathbf{x}_k is the estimate of the optimal solution \mathbf{x}^* and $f(\mathbf{x}_k)$ is the estimate of the optimal value of (5), $f(\mathbf{x}^*)$, at iteration k . We write the linearization of the function f at \mathbf{x}_k and denote it

as h_k :

$$h_k(s) = f(x_k) + \langle \nabla f(x_k), s - x_k \rangle \quad (6)$$

where s is a vector of \mathbb{R}^n , $\nabla f(x_k)$ is the gradient of f at x_k and $\langle \cdot, \cdot \rangle$ denotes the dot product between two vectors of \mathbb{R}^n .

↪ **Step 1.** The first step of the FW algorithm at iteration k consists of finding a minimizer $s_k \in \mathcal{D}$ of h_k on the convex set \mathcal{D} (line 2 in Alg. 1). Such a vector s_k is called a *support vector* of \mathcal{D} or simply a *support* and is defined as follows:

$$s_k \in \arg \min_{s \in \mathcal{D}} h_k(s) = \arg \min_{s \in \mathcal{D}} \langle \nabla f(x_k), s \rangle. \quad (7)$$

Fig. 3 gives a graphical understanding of support s_k . The vector s_k belongs to \mathcal{D} and is in the *most* opposite direction w.r.t. $\nabla f(x_k)$. In order to highlight the importance of the direction in which a support s_k is computed, we now introduce the notion of *support direction* and *support function*. Given a support direction $d \in \mathbb{R}^n$, the support function $S_{\mathcal{D}}$ returns a set of \mathcal{D} and is defined as:

$$S_{\mathcal{D}}(d) = \arg \min_{s \in \mathcal{D}} \langle d, s \rangle \subset \mathcal{D}. \quad (8)$$

The support function $S_{\mathcal{D}}$ may return a set with more than one vector. We only need to use one vector of this set. Thinking in terms of the direction of support allows us to understand that this direction can be rescaled while preserving the output of the support function:

$$\forall d \in \mathbb{R}^n, \forall \alpha > 0, S_{\mathcal{D}}(\alpha d) = S_{\mathcal{D}}(d). \quad (9)$$

A support $s_k \in \mathcal{D}$ at iteration k is thus computed in the direction $d_k = \nabla f(x_k)$ and belongs to $S_{\mathcal{D}}(\nabla f(x_k))$, $s_k \in S_{\mathcal{D}}(\nabla f(x_k))$.

We now explain how to compute the support vector s_k in the case of the distance computation problem (4) where we minimize $f(x) = \|x\|^2$ on the Minkowski difference \mathcal{D} of \mathcal{A}_1 and \mathcal{A}_2 . First, we have $\nabla f(x) = 2x$. Therefore, in the case of problem (4), it follows that:

$$s_k \in S_{\mathcal{D}}(x_k) = \arg \min_{s \in \mathcal{D}} \langle x_k, s \rangle. \quad (10)$$

As demonstrated by [12], any vector $s \in S_{\mathcal{D}}(d)$ related to the Minkowski difference can be decomposed as the difference between two support vectors $s_{\mathcal{A}_1} \in S_{\mathcal{A}_1}(d)$ and $s_{\mathcal{A}_2} \in S_{\mathcal{A}_2}(-d)$ over the two individual shapes, leading to the following relation:

$$s = s_{\mathcal{A}_1} - s_{\mathcal{A}_2} \in S_{\mathcal{D}}(d). \quad (11)$$

Equation (11) shows that we can construct a support of the Minkowski difference from the supports of the original shapes. This property highlights the powerful change of perspective of working on the Minkowski difference. Indeed, there exists a large number of shapes for which computing supports is simple: spheres, ellipsoids, cylinders, capsules, polytopes etc. [7], [21], [26]. Fig. 4 illustrates the construction of a support of the Minkowski difference \mathcal{D} using the supports of the original shapes \mathcal{A}_1 and \mathcal{A}_2 .

↪ **Step 2.** Once a support vector $s_k \in S_{\mathcal{D}}(x_k)$ has been computed, we update the iterate x_k to obtain x_{k+1} by taking a convex combination between s_k and x_k . The original FW algorithm uses a parameter-free update:

$$x_{k+1} = \gamma_k x_k + (1 - \gamma_k) s_k, \quad (12)$$

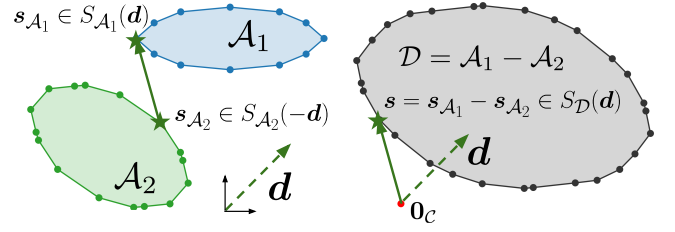


Fig. 4. Computing a support vector on the Minkowski difference using support vectors (represented by star shapes in the drawing) on the individual shapes. The vector $s_{\mathcal{A}_1}$ is a support vector of shape \mathcal{A}_1 in direction d . The vector $s_{\mathcal{A}_2}$ is a support vector of shape \mathcal{A}_2 in direction $-d$. The constructed vector $s = s_{\mathcal{A}_1} - s_{\mathcal{A}_2}$ is a support vector of the Minkowski difference \mathcal{D} in the direction d .

where $\gamma_k = \frac{k+1}{k+2} \in [0, 1]$ controls the step size. Alternatively, a line search can be carried out to find a better iterate x_{k+1} (line 4 in Alg. 1):

$$\begin{aligned} \gamma_k &= \arg \min_{\gamma \in [0, 1]} f(\gamma x_k + (1 - \gamma) s_k) \\ x_{k+1} &= \gamma_k x_k + (1 - \gamma_k) s_k. \end{aligned} \quad (13)$$

In the distance computation case where $f(x) = \|x\|^2$, this linesearch (13) is equivalent to projecting 0_C onto the segment $[x_k, s_k]$, $x_k = \text{proj}_{[x_k, s_k]}(0_C)$ (line 4 in Alg. 1). Since \mathcal{D} is convex, both (12) and (13) updates are guaranteed to remain in \mathcal{D} .

Stopping criteria. As Frank-Wolfe deals with convex problems, the *duality gap* associated with problem (5) can be used as a stopping criterion. Due to its convexity, the function f is always above its linearization. Otherwise said, for any $x \in \mathbb{R}^n$ and any $s \in \mathbb{R}^n$:

$$f(s) \geq f(x) + \langle \nabla f(x), s - x \rangle. \quad (14)$$

Reworking this inequality and applying the min operator enables us to compute the Frank-Wolfe duality gap $g_{\text{FW}}(x) \in \mathbb{R}_+$ which gives an upper-bound on the difference $f(x) - f(x^*)$:

$$f(x) - f(x^*) \leq -\min_{s \in \mathcal{D}} \langle \nabla f(x), s - x \rangle = g_{\text{FW}}(x). \quad (15)$$

In particular, at iteration k of the FW algorithm, we have:

$$f(x_k) - f(x^*) \leq g_{\text{FW}}(x_k) = \langle \nabla f(x_k), x_k - s_k \rangle, \quad (16)$$

where $s_k \in S_{\mathcal{D}}(\nabla f(x_k))$ is the support vector computed at iteration k in the direction of $\nabla f(x_k)$. The duality-gap $g_{\text{FW}}(x_k)$ serves as a convergence criterion for the Frank-Wolfe method and is cheap to compute. Applied to the distance computation problem (4), the duality gap at iteration k , $g_{\text{FW}}(x_k)$, guarantees that:

$$\|x_k\|^2 - \|x^*\|^2 \leq g_{\text{FW}}(x_k) = 2 \langle x_k, x_k - s_k \rangle. \quad (17)$$

Using the triangular inequality of the Euclidian norm and the convexity of the Minkowski difference \mathcal{D} , we can show that:

$$\|x_k - x^*\|^2 \leq \|x_k\|^2 - \|x^*\|^2 \leq g_{\text{FW}}(x_k). \quad (18)$$

Inequality (18) is useful in practice as it allows the fine control of the desired tolerance on the distance to the optimal solution x^* (line 3 in Alg. 1). Indeed, if one wants to compute an estimate x of the optimal solution x^* at precision ϵ ,

Algorithm 2 Boolean collision checking: separating plane condition

Insert after line 2 in Alg. 1:

```

1: If  $\max(0, \langle \mathbf{d}_k / \|\mathbf{d}_k\|, \mathbf{s}_k \rangle) > \epsilon_{\text{col}}$ , return False
   If after termination  $d_{1,2} \leq \epsilon_{\text{col}}$ , return True, otherwise
   return False.

```

meaning that $\|\mathbf{x} - \mathbf{x}^*\| \leq \sqrt{\epsilon}$, it is sufficient to check that $g_{\text{FW}}(\mathbf{x}) \leq \epsilon$.

Boolean collision checking. As mentioned earlier, the problem of distance computation encompasses the problem of collision checking. Indeed, in collision checking, we are only interested in finding a separating plane between \mathcal{A}_1 and \mathcal{A}_2 , if it exists. This is equivalent to finding a separating plane between \mathcal{D} and $\mathbf{0}_{\mathcal{C}}$. For any support direction \mathbf{d} , if we have:

$$\langle \mathbf{d}, \mathbf{s} \rangle > 0, \mathbf{s} \in S_{\mathcal{D}}(\mathbf{d}), \quad (19)$$

then the plane supported by the vector \mathbf{d} separates \mathcal{D} from $\mathbf{0}_{\mathcal{C}}$ [21]. This also means that, in the case where the two shapes intersect, collision checking has the same computational complexity as distance computation. In general, at iteration k , the value $\max(0, \langle \mathbf{d}_k / \|\mathbf{d}_k\|, \mathbf{s}_k \rangle)$ is a lower bound on the distance between the shapes, $\text{dist}(\mathcal{A}_1, \mathcal{A}_2)$, and it can be used as a stopping criterion in the boolean collision check. As soon as the lower bound on $\text{dist}(\mathcal{A}_1, \mathcal{A}_2)$ is guaranteed to be positive, the algorithm can be stopped. Otherwise, the algorithm continues until the stopping criterion defined by (18) is met. As shown in Alg. 2, we add this separating plane condition before line 2 in Alg. 1. The condition on the lower bound of $\text{dist}(\mathcal{A}_1, \mathcal{A}_2)$ is met relative to a threshold ϵ_{col} . This threshold sets at what distance the shapes are considered to be in collision and depends on the application. In practice, since we use double-precision floats in our benchmarks (see Sec. IV), the test on the lower bound of $\text{dist}(\mathcal{A}_1, \mathcal{A}_2)$ can be computed down to machine precision. This means the distance computation threshold ϵ can take values down to 10^{-12} in (18). This corresponds to a precision on the distance between shapes on the order of micro-meters ($\sqrt{\epsilon} = 10^{-6}\text{m}$). In robotics applications where the entire pipeline is no more precise than millimeters, it is often sufficient to consider that below a threshold of 10^{-4}m (i.e $\epsilon = 10^{-8}$) the shapes are in collision; above that threshold the shapes are not in collision. In our applications, we use $\epsilon_{\text{col}} = \sqrt{\epsilon}$.

Computing support vector on meshes. While the support vector of basic primitives (sphere, ellipsoid, box, etc.) presents closed-form solutions, this is not the case for meshes. In the case of convex meshes, an efficient approach for computing the support direction of meshes is the *hill-climbing* algorithm [26], which allows retrieving the supporting vertex or face of the meshes thanks to a simple neighbor-descent procedure. Yet, this procedure is sensitive to the initial-guess solution. By leveraging Nesterov and Polyak acceleration schemes introduced in Sec. III, which both tend to reduce the oscillations hindered by gradient-descent type algorithms, we show in

Algorithm 3 Frank-Wolfe algorithm with line-search (see Alg. 1) rewritten with active-sets and applied to the distance computation problem (4)

Let $\mathbf{x}_0 \in \mathcal{D}$, $W_0 = \{\mathbf{x}_0\}$, $\epsilon > 0$

For $k=0, 1, \dots$ **do**

```

1:  $\mathbf{d}_k = \mathbf{x}_k$  ▷ Direction of support
2:  $\mathbf{s}_k \in S_{\mathcal{D}}(\mathbf{d}_k)$  ▷ Support (8)
3: If  $g_{\text{FW}}(\mathbf{x}_k) \leq \epsilon$ , return  $f(\mathbf{x}_k)$  ▷ Duality gap (16)
4:  $\widetilde{W}_{k+1} = W_k \cup \{\mathbf{s}_k\}$  ▷ Augment active-set
5:  $\mathbf{x}_{k+1} = \text{proj}_{\text{conv}(\widetilde{W}_{k+1})}(\mathbf{0}_{\mathcal{C}})$  ▷ Project  $\mathbf{0}_{\mathcal{C}}$  on  $\text{conv}(\widetilde{W}_{k+1})$ 
6:  $W_{k+1} = \{\mathbf{x}_{k+1}\}$  ▷ Update active-set

```

Sec. IV that this helps the hill-climbing algorithm to perform less iterations in practice, leading to faster computation times.

The Frank-Wolfe active-set. As with many gradient-descent algorithms, the FW method tends to zig-zag towards the optimal solution [40], slowing down the convergence to the optimum. This behavior is undesired and amplified if the optimal solution \mathbf{x}^* lies close to the boundary of the constraint set \mathcal{D} . In collision detection, this corresponds to the case where the two shapes are not intersecting. This zig-zagging behavior is due to the way that Frank-Wolfe approaches the set of active constraints [40], also called *active-set* in the optimization literature [44]. In the FW setting, the active set at iteration k , denoted $W_k = \{\mathbf{s}^0, \dots, \mathbf{s}^r\} \subset \mathcal{D}$, is the set of vectors in \mathcal{D} used by the algorithm to maintain a convex combination of the iterate \mathbf{x}_k :

$$\mathbf{x}_k = \sum_{i=0}^r \lambda^i \mathbf{s}^i, \sum_{i=0}^r \lambda^i = 1 \text{ with } \mathbf{s}^i \in W_k \subset \mathcal{D} \text{ and } \lambda^i > 0. \quad (20)$$

In Alg. 3, we rewrite the FW algorithm with line search (Alg. 1) in order to highlight the notion of active set:

- At iteration k , the active-set is only composed of \mathbf{x}_k , $W_k = \{\mathbf{x}_k\}$.
- The active-set W_k is then augmented by computing a support \mathbf{s}_k (line 2 in Alg. 3) to obtain $\widetilde{W}_{k+1} = \{\mathbf{x}_k, \mathbf{s}_k\}$ (line 4 in Alg. 3).
- We then minimize function f on the convex-hull of \widetilde{W}_{k+1} , $\text{conv}(\widetilde{W}_{k+1})$, which is simply the segment $[\mathbf{x}_k, \mathbf{s}_k]$. For the distance computation problem (4), this linesearch operation is equivalent to projecting $\mathbf{0}_{\mathcal{C}}$ onto the segment $[\mathbf{x}_k, \mathbf{s}_k]$ (line 5 in Alg. 3).
- Finally, the active-set is updated $W_{k+1} = \{\mathbf{x}_{k+1}\}$ (line 6 in Alg. 3).

In practice, discarding previously computed supports when updating the active set is inefficient and causes the zig-zagging phenomenon observed in the FW algorithm [40]. In the optimization literature, a rich and wide variety of variants of the FW algorithm have been introduced to efficiently cope with the active set in order to improve the convergence rate of the FW method [34], [36], [37], [45], [46]. However, these variants remain too generic and are not suited for the specific problem of collision detection. In the following, we propose instead incorporating the active-set strategy used in GJK within the Frank-Wolfe setting.

Connection between GJK and Frank-Wolfe. In the case of collision detection, [12] developed an efficient strategy to handle the active set at a minimal cost. To represent the current estimate \mathbf{x}_k and the optimal solution \mathbf{x}^* , GJK exploits the concept of *simplexes* in \mathbb{R}^3 . A simplex in \mathbb{R}^n corresponds to a set containing *at most* $n + 1$ vectors of \mathbb{R}^n , and the *rank* r of a simplex is the number of vectors it contains ($0 < r \leq n + 1$). For 3-dimensional spaces, a simplex corresponds either to a point ($r = 1$), a segment ($r = 2$), a triangle ($r = 3$), or a tetrahedron ($r = 4$). Similarly to the simplex methods for Linear Programming [47], the Carathéodory theorem [48] motivates the use of simplexes. Let \mathcal{Y} be a set of $N \geq n$ vectors in \mathbb{R}^n , $\mathcal{Y} = \{\mathbf{y}^i \in \mathbb{R}^n\}_{0 \leq i \leq N}$. The Carathéodory theorem states that any vector $\mathbf{x} \in \text{conv}(\mathcal{Y})$ can be expressed as the convex combination of at most $n + 1$ vectors of \mathcal{Y} :

$$\mathbf{x} = \sum_{j=0}^r \lambda^j \mathbf{y}^j, \text{ with } \mathbf{y}^j \in \mathcal{Y}, \lambda^j > 0, \sum_{i=0}^r \lambda^i = 1. \quad (21)$$

Hence, any vector in \mathcal{D} , and particularly the optimal solution $\mathbf{x}^* \in \mathcal{D} = \text{conv}(\mathcal{D})$ of the distance computation problem (4), can be identified as a convex combination of the vectors composing a simplex W . Relying on simplexes is attractive as there is no need to run any algorithm to compute the convex hull of a simplex as they are convex by construction. Frank-Wolfe algorithms may operate on more complex active sets, which might become hard to tackle from a computational point of view [38], [40]. In other words, the problem of finding the optimal solution \mathbf{x}^* can be reformulated as the problem of identifying the optimal simplex W^* on which \mathbf{x}^* can be decomposed into a convex combination. This is precisely the approach followed by GJK that we now detail as well as illustrate in Fig. 5.

At iteration k of GJK, the current iterate \mathbf{x}_k is a convex combination of the vectors composing the simplex W_k of rank $r_k \leq n$. This corresponds to Fig. 5a. To update \mathbf{x}_k and W_k , the following procedure is applied:

- After computing support vector \mathbf{s}_k (line 2 in Alg. 3, illustrated in Fig. 5b), we add \mathbf{s}_k to W_k to obtain $\widetilde{W}_{k+1} = W_k \cup \{\mathbf{s}_k\}$ (line 4 in Alg. 3). The set \widetilde{W}_{k+1} is now a simplex of rank $\widetilde{r}_{k+1} \leq n + 1$, as shown in Fig. 5c.
- We then minimize function $f(\mathbf{x}) = \|\mathbf{x}\|^2$ on \widetilde{W}_{k+1} to obtain \mathbf{x}_{k+1} , corresponding to projecting $\mathbf{0}_C$ onto \widetilde{W}_{k+1} : $\mathbf{x}_{k+1} = \text{proj}_{\text{conv}(\widetilde{W}_{k+1})}(\mathbf{0}_C)^1$ (line 5 in Alg. 3). This projection is illustrated in figures 5c and 5d.
- We then have two cases, summarized in Alg 4:
 - 1) If $\mathbf{x}_{k+1} = \mathbf{0}_C$, the algorithm is stopped. Thus, we have $\mathbf{x}^* = \mathbf{0}_C$ and $d_{1,2} = 0$ in (4) (line 1 in Alg. 4).
 - 2) Otherwise, we construct W_{k+1} from \widetilde{W}_{k+1} . To do so, we retain only the minimal number of vectors in \widetilde{W}_{k+1} needed to express \mathbf{x}_{k+1} as a convex combination (line 2 in Alg. 4). Indeed, as $\mathbf{0}_C \notin \widetilde{W}_{k+1}$, the projection \mathbf{x}_{k+1} of $\mathbf{0}_C$ on \widetilde{W}_{k+1} necessarily lies on a face of \widetilde{W}_{k+1} , and can be expressed as

¹The efficient projection onto simplexes in \mathbb{R}^3 , named the *distance sub-algorithm* by [12], is thoroughly covered in [7], [21] and its robustness is improved in [30].

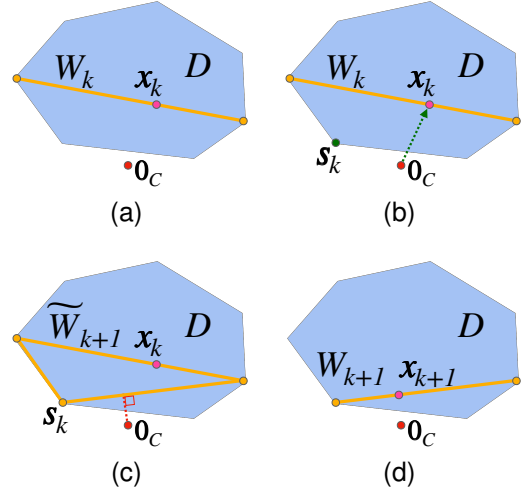


Fig. 5. Illustration of the GJK simplex strategy in 2D: (a) beginning of the k^{th} iteration, (b) support point computation, (c) simplex augmentation, (d) simplex update.

Algorithm 4 Fully-corrective FW using simplexes, applied to the distance computation problem (4). This algorithm is identical to GJK [12]

In Alg. 3, let $W_0 = \emptyset$ and replace line 6 by:

- 1) **If** $\mathbf{x}_{k+1} = \mathbf{0}_C$, **return** 0
If the algorithm has not terminated, update \widetilde{W}_{k+1} to retain only the smallest number of vectors needed to express \mathbf{x}_{k+1} .
- 2) $W_{k+1} = \{\mathbf{s}^1, \dots, \mathbf{s}^r\}$ where $\mathbf{s}^1, \dots, \mathbf{s}^r$ are the smallest number of vectors in \widetilde{W}_{k+1} such that \mathbf{x}_{k+1} is a convex combination of $\mathbf{s}^1, \dots, \mathbf{s}^r$.

a convex combination of the vectors composing this face. This ensures that W_{k+1} is necessarily of rank $r_{k+1} < \widetilde{r}_{k+1} \leq n + 1$. For example, Fig. 5d shows the result of the simplex update obtained in Fig. 5c.

Through this discussion, it is clear that GJK is a particular case of Frank-Wolfe. More specifically, it is a sub-case of the fully-corrective Frank-Wolfe algorithm analyzed by [40]. The strategy used by GJK to handle the active set has proved to be very efficient in practice and renders the GJK algorithm state-of-the-art for collision detection. In the next section, we propose to leverage the formulation of collision detection as a Frank-Wolfe sub-case to accelerate its convergence following the well-established Polyak and Nesterov acceleration paradigm [41].

III. ACCELERATING COLLISION DETECTION

Gradient descent (GD) is the backbone of many convex optimization methods and relies solely on the gradient of the objective function. Second-order methods [44], such as Newton methods, have faster convergence rates than GD at the price of requiring the computation and the inversion of Hessian quantities. Momentum methods have thus been introduced in the optimization literature to provide gradient-based

methods with improved convergence rates without requiring costly Hessian evaluation. In this section, we use recent work linking the *Polyak* and *Nesterov* accelerations of GD to the FW algorithm [13], [14] to globally accelerate collision detection. These global accelerations of collision detection are experimentally evaluated in Sec. IV on several benchmarks.

A. Background on acceleration methods in convex optimization

Polyak acceleration for unconstrained optimization. We initially consider the following *unconstrained* minimization problem:

$$f(x^*) = \min_{x \in \mathbb{R}^n} f(x), \quad (22)$$

where $f : \mathbb{R}^n \rightarrow \mathbb{R}$ is a convex and differentiable function. The vanilla gradient-descent algorithm follows the slope of f given by its gradient ∇f . The following scheme is applied iteratively until a given convergence criterion is met (e.g., $\|\nabla f(x_k)\| < \epsilon$, with ϵ being the desired precision):

$$x_{k+1} = x_k + \alpha_k \nabla f(x_k), \quad (23)$$

where $x_k \in \mathbb{R}^n$ is the current iterate and $\alpha_k \in \mathbb{R}$ is the gradient step. This standard setting leads to a simple implementation with linear convergence rate ($O(1/k)$).

To go beyond this linear convergence regime, acceleration techniques have been devised in the optimization community to provide quadratic convergence rate ($O(1/k^2)$) or more [35], by relying on relatively cheap gradient evaluations. Among these gradient-descent acceleration techniques, the Polyak (or Heavy-Ball) [49] and Nesterov acceleration [41] are two of the better-studied and most popular in practice [35]. These techniques are based on accumulating previously computed gradients in a *momentum* term d_k and using this momentum d_k to update the current iterate x_k . The Polyak update scheme for unconstrained gradient descent is illustrated in Fig. 6a and goes as follows:

$$d_k = \delta_k d_{k-1} + \alpha_k \nabla f(x_k) \quad (24a)$$

$$x_{k+1} = x_k + d_k, \quad (24b)$$

where schemes $\delta_k \in \mathbb{R}$ is the momentum parameter. The role of momentum d_k is to smooth the trajectory of iterates converging towards the optimum by geometrically averaging previously computed gradients. The δ_k momentum parameter is selected to prevent damping or overshooting of the iterate trajectory when going towards the optimal solution x^* .

Nesterov acceleration for unconstrained optimization. The Nesterov update scheme is the second most well-known method for accelerating unconstrained gradient descent and it is only a slight modification on top of the Polyak scheme. Contrary to the Polyak case, in the Nesterov acceleration scheme the current iterate x_k is extrapolated using the momentum term d_k to compute the intermediary vector $y_k = x_k + \delta_k d_k$. The gradient is then computed at the vector y_k . The Nesterov

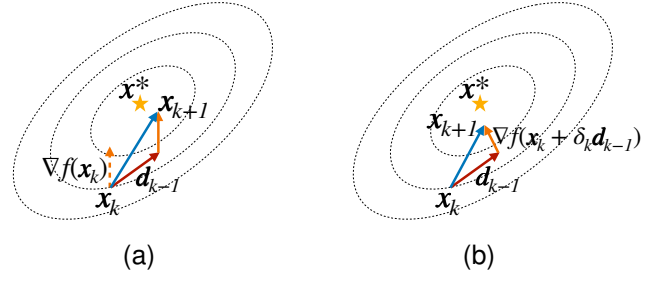


Fig. 6. (a) Polyak and (b) Nesterov acceleration schemes for unconstrained gradient descent. The gradient descent algorithm aims at finding the optimum x^* by following the slope given by the gradient of function f , ∇f . The vector d_{k-1} is the momentum accumulated over the optimization trajectory. The two schemes differ in where the gradient is computed at iteration k ; the Nesterov scheme introduces an intermediary point $y_k = x_k + \delta_k d_{k-1}$ to compute the gradient.

update scheme for unconstrained gradient descent is illustrated in Fig. 6b and goes as:

$$y_k = x_k + \delta_k d_{k-1} \quad (25a)$$

$$d_k = \delta_k d_{k-1} + \alpha_k \nabla f(y_k) \quad (25b)$$

$$x_{k+1} = x_k + d_k \quad (25c)$$

where δ_k is the momentum parameter as in the Polyak scheme, and $y_k \in \mathbb{R}^n$ is an intermediary quantity. Computing the term y_k leads to an anticipatory behavior in similar spirit to extra-gradient methods [35].

Accelerating the Frank-Wolfe algorithm with Polyak and Nesterov. Recent works of [13], [14] have proposed to adapt the Polyak and Nesterov accelerations to the FW setting. We propose to leverage and adapt this FW acceleration scheme to the context of collision detection, by notably extending the FW formulation of collision detection previously developed in Sec. II.

In the original FW algorithm, the support vector at iteration k , s_k , is computed in the direction of the gradient $\nabla f(x_k)$ (line 1 in Alg. 1). In the Polyak acceleration of FW proposed by [13], the direction of support for computing s_k is instead defined by:

$$d_k = \delta_k d_{k-1} + (1 - \delta_k) \nabla f(x_k) \quad (26a)$$

$$s_k = S_{\mathcal{D}}(d_k), \quad (26b)$$

where $\delta_k = \frac{k+1}{k+3} \in [0, 1]$ is the momentum parameter and $S_{\mathcal{D}}$ is the support function as defined in (8). In the Nesterov acceleration of FW proposed by [14], the direction of support for computing s_k is slightly different from the Polyak scheme (26) as it introduces y_k , an intermediary vector as in the GD Nesterov scheme (25) in order to evaluate the gradient $\nabla f(y_k)$:

$$y_k = \delta_k x_k + (1 - \delta_k) s_{k-1} \quad (27a)$$

$$d_k = \delta_k d_{k-1} + (1 - \delta_k) \nabla f(y_k) \quad (27b)$$

$$s_k = S_{\mathcal{D}}(d_k), \quad (27c)$$

where s_{k-1} is the support vector computed at the previous iteration. To ensure y_k stays in \mathcal{D} , it is a convex combination of x_k and s_{k-1} , both vectors of \mathcal{D} . The direction of support is then obtained by taking a convex combination of the previous

Algorithm 5 Polyak-accelerated and Nesterov-accelerated Frank-Wolfe [13], [14]

In Alg. 1 and Alg. 3, let $\mathbf{d}_{-1} = \mathbf{s}_{-1} = \mathbf{x}_0$, $\delta_k = \frac{k+1}{k+3}$ and replace line 1 by:

$$\begin{aligned} 1: \mathbf{y}_k &= \begin{cases} \mathbf{x}_k & \text{Polyak} \\ \delta_k \mathbf{x}_k + (1 - \delta_k) \mathbf{s}_{k-1} & \text{Nesterov} \end{cases} \\ 2: \mathbf{d}_k &= \delta_k \mathbf{d}_{k-1} + (1 - \delta_k) \nabla f(\mathbf{y}_k) \end{aligned}$$

support direction \mathbf{d}_{k-1} and the gradient $\nabla f(\mathbf{y}_k)$. Both the Polyak and Nesterov accelerations of Frank-Wolfe are summed up in Alg. 5.

The works [13], [14] have experimentally shown that these accelerations strategies lead to a better convergence rate of the FW algorithm when compared to the original FW algorithm. In the following, we explain how to adapt the Polyak and Nesterov accelerations of FW to collision detection.

B. Acceleration of collision detection and distance computation

Adapting Nesterov and Polyak fully-corrective Frank-Wolfe to distance computation. Preserving GJK's simplex strategy is crucial for collision detection as it greatly speeds up the vanilla FW algorithm. Therefore, we adapt (26) and (27) accordingly as:

$$\mathbf{y}_k = \begin{cases} \mathbf{x}_k & \text{if Polyak} \\ \delta_k \mathbf{x}_k + (1 - \delta_k) \mathbf{s}_{k-1} & \text{if Nesterov} \end{cases} \quad (28a)$$

$$\mathbf{d}_k = \delta_k \mathbf{d}_{k-1} + (1 - \delta_k) \nabla f(\mathbf{y}_k) \quad (28b)$$

$$\mathbf{s}_k = S_{\mathcal{D}}(\mathbf{d}_k), \quad (28c)$$

$$\widetilde{W}_{k+1} = W_k \cup \{\mathbf{s}_k\}, \quad (28d)$$

$$\mathbf{x}_{k+1} = \text{proj}_{\text{conv}(\widetilde{W}_{k+1})}(\mathbf{0}_C). \quad (28e)$$

These steps are also summarized in Alg. 6. The update of simplex W_{k+1} from \widetilde{W}_{k+1} is then identical to the one described in Alg. 4. The original duality gap defined in Sec. II (Eq. 16) can no longer be used as a convergence criterion. Indeed, the following inequality:

$$\|\mathbf{x}_k - \mathbf{x}^*\|^2 \leq g_{\text{FW}}(\mathbf{x}_k) = 2\langle \mathbf{x}_k, \mathbf{x}_k - \mathbf{s}_k \rangle, \mathbf{s}_k \in S_{\mathcal{D}}(\mathbf{x}_k),$$

is no longer valid because the support vector \mathbf{s}_k is no longer computed in the direction of the gradient $\nabla f(\mathbf{x}_k) = 2\mathbf{x}_k$. Next we will show that the original stopping criterion devised in Sec. II cannot be used and we need to derive a new one.

Stopping criterion. As the number of iteration k increases, $\delta_k \xrightarrow{k \rightarrow \infty} 1$ in (28). Therefore, \mathbf{d}_k tends to be equal to \mathbf{d}_{k-1} (28b) and thus $\mathbf{s}_k = \mathbf{s}_{k-1}$ (28c). As a consequence, augmenting W_k with \mathbf{s}_k to construct \widetilde{W}_{k+1} (see (28d)) and then projecting $\mathbf{0}_C$ onto \widetilde{W}_{k+1} (28e) will not result in any progress. Therefore, $\mathbf{x}_{k+1} = \mathbf{x}_k$: the algorithm reaches a fixed point and is stuck on constant support direction \mathbf{d} .

In order to cope with this issue, we use the following strategy. Suppose $\mathbf{x}_k \neq \mathbf{0}_C$. Since $\mathbf{x}_k = \text{proj}_{\text{conv}(W_k)}(\mathbf{0}_C)$ we have:

$$\forall \mathbf{s}^i \in W_k, \langle \mathbf{x}_k, \mathbf{x}_k - \mathbf{s}^i \rangle = 0. \quad (29)$$

Algorithm 6 Polyak and Nesterov-accelerated GJK

Let $\mathbf{x}_0 \in \mathcal{D}$, $W_0 = \emptyset$, $\mathbf{d}_{-1} = \mathbf{s}_{-1} = \mathbf{x}_0$, $\epsilon > 0$

For $k=0, 1, \dots$ do

- 1: $\delta_k = \frac{k+1}{k+3}$ ▷ Momentum parameter value
- 2: $\mathbf{y}_k = \begin{cases} \mathbf{x}_k & \text{Polyak} \\ \delta_k \mathbf{x}_k + (1 - \delta_k) \mathbf{s}_{k-1} & \text{Nesterov} \end{cases}$ ▷ Intermediary point (28a)
- 3: $\mathbf{d}_k = \delta_k \mathbf{d}_{k-1} + (1 - \delta_k) \nabla f(\mathbf{y}_k)$ ▷ Support dir. (28b)
- 4: $\mathbf{s}_k \in S_{\mathcal{D}}(\mathbf{d}_k)$ ▷ Support (8)
- 5: **if** $g(\mathbf{x}_k) \leq \epsilon$ **then** ▷ Fixed-point condition (32)
- 6: **if** $\mathbf{d}_k = \mathbf{x}_k$, **return** $f(\mathbf{x}_k)$ ▷ Algorithm terminates
- 7: $\mathbf{s}_k \in S_{\mathcal{D}}(\nabla f(\mathbf{x}_k))$ ▷ Compute \mathbf{s}_k in dir. $\nabla f(\mathbf{x}_k)$
- Replace line 3 by: $\mathbf{d}_k = \mathbf{x}_k$ until termination.**
- 8: $\widetilde{W}_{k+1} = W_k \cup \{\mathbf{s}_k\}$ ▷ Augment active-set
- 9: $\mathbf{x}_{k+1} = \text{proj}_{\text{conv}(\widetilde{W}_{k+1})}(\mathbf{0}_C)$ ▷ Project $\mathbf{0}_C$ on $\text{conv}(\widetilde{W}_{k+1})$
- 10: **if** $\mathbf{x}_{k+1} = \mathbf{0}_C$, **return** 0
- 11: $W_{k+1} = \{\mathbf{s}^1, \dots, \mathbf{s}^r\}$ where $\mathbf{s}^1, \dots, \mathbf{s}^r$ are the smallest number of vectors in \widetilde{W}_{k+1} such that \mathbf{x}_{k+1} is a convex combination of $\mathbf{s}^1, \dots, \mathbf{s}^r$.

After computing $\mathbf{s}_k \in S_{\mathcal{D}}(\mathbf{d}_k)$, if we have:

$$\langle \mathbf{x}_k, \mathbf{x}_k - \mathbf{s}_k \rangle \neq 0, \quad (30)$$

then \mathbf{s}_k is not a linear combination of vectors in W_k . Therefore, augmenting \widetilde{W}_k with \mathbf{s}_k to obtain \widetilde{W}_{k+1} and projecting $\mathbf{0}_C$ onto $\text{conv}(\widetilde{W}_{k+1})$ to obtain \mathbf{x}_{k+1} will result in the algorithm progressing toward the optimum \mathbf{x}^* . Suppose on the contrary that:

$$\langle \mathbf{x}_k, \mathbf{x}_k - \mathbf{s}_k \rangle = 0, \quad (31)$$

then \mathbf{s}_k is a linear combination of vectors in W_k . Adding \mathbf{s}_k to W_k will thus not result in any progress towards the optimum. As a consequence, Eq. (31) encompasses two cases:

- If the support direction \mathbf{d}_k is aligned with $\nabla f(\mathbf{x}_k)$, Eq. (31), corresponding to $g_{\text{FW}}(\mathbf{x}_k) = 0$, matches the termination criterion of the distance computation problem and therefore we have reached the optimum i.e $\mathbf{x}_k = \mathbf{x}^*$.
- Otherwise, if \mathbf{d}_k is not aligned with $\nabla f(\mathbf{x}_k)$, the algorithm cannot stop as a null duality gap is not met. The algorithm thus enters a cycle where it iterates until Eq. (31) does not hold. To cope with this undesired behavior we simply stop the Polyak or the Nesterov acceleration as soon as Eq. (31) is met and switch back to the non-accelerated version Alg. 4.

We thus define the function g such that for any $\mathbf{s}_k \in \mathcal{D}$:

$$g(\mathbf{x}_k) = 2\langle \mathbf{x}_k, \mathbf{x}_k - \mathbf{s}_k \rangle, \quad (32)$$

g is used in Alg. 6 as an optimality criterion ($g \leq \epsilon$) either for stopping the Polyak and Nesterov accelerations in order to continue with the vanilla GJK, or as stopping criteria qualifying an optimal solution, in which case $g = g_{\text{FW}}$ and (18) holds. The entire algorithm is summarized in Alg. 6.

Nesterov acceleration for non-strictly convex shapes. Let us explain the effect of the Nesterov acceleration on the support

Algorithm 7 Normalize direction for non-strictly convex shapes in Nesterov-accelerated GJK

Replace line 3 in Alg. 6 by:

$$1: \mathbf{d}_k = \delta_k \frac{\mathbf{d}_{k-1}}{\|\mathbf{d}_{k-1}\|} + (1 - \delta_k) \frac{\nabla f(\mathbf{y}_k)}{\|\nabla f(\mathbf{y}_k)\|}$$

direction update (28b) and distinguish between strictly convex and non-strictly convex \mathcal{D} :

- If \mathcal{D} is strictly convex, any vector \mathbf{s} belonging to the surface of \mathcal{D} has a unique corresponding direction \mathbf{d} such that $\mathbf{s} = S_{\mathcal{D}}(\mathbf{d})$. Here, we stress the fact that the support function $S_{\mathcal{D}}$ returns only *one* vector. Consequently, we have $\mathbf{d}_k \neq \mathbf{d}_{k-1}$ and therefore $\mathbf{s}_k \neq \mathbf{s}_{k-1}$. The fixed point condition (31) is thus not met unless $\delta_k = 1$ and Nesterov acceleration continues to be applied in Alg. 6. In practice, the algorithm runs until δ_k gets close to 1 or \mathbf{x}_k gets close to $\mathbf{0}_C$. The condition (31) is then satisfied as the algorithm starts to cycle. The Nesterov acceleration is thus removed and the algorithm runs until the convergence criteria is satisfied, guaranteed by the Frank-Wolfe algorithm.
- Otherwise, if \mathcal{D} is non-strictly convex, multiple support directions $\{\mathbf{d}^1, \dots, \mathbf{d}^m, \dots\}$ can yield the same support vector $\mathbf{s} \in S_{\mathcal{D}}(\mathbf{d}^1) = \dots = S_{\mathcal{D}}(\mathbf{d}^m) = \dots$ etc. Consequently, it is possible to have $\mathbf{d}_{k-1} \neq \mathbf{d}_k$ and $\mathbf{s}_k = \mathbf{s}_{k-1}$. Therefore, even though δ_k is not close to 1, the fixed point condition (31) can be verified. The Nesterov acceleration is stopped, possibly prematurely.

The latter case is especially problematic when shapes \mathcal{A}_1 and \mathcal{A}_2 are in close-proximity, which is ultimately the type of collision problems commonly encountered in simulation or motion planning with contacts. In (28b), this is due to the norm of $\nabla f(\mathbf{y}_k)$ being predominant over the norm of \mathbf{d}_{k-1} as k increases, $\|\mathbf{d}_{k-1}\| \ll \|\nabla f(\mathbf{y}_k)\|$. As a consequence, the Nesterov acceleration enters a cycle: the support direction \mathbf{d}_k does not change enough compared to \mathbf{d}_{k-1} , hence the support point \mathbf{s}_k is identical to \mathbf{s}_{k-1} and therefore the intermediary point \mathbf{y}_k does not change and the cycle repeats. As a consequence, the criterion (31) is met and the Nesterov acceleration is stopped to escape the cycle, possibly prematurely. To prevent this phenomenon observed on non-strictly convex \mathcal{D} , we propose to replace (28b) by a simple heuristic which normalizes the gradient and momentum directions as follows:

$$\mathbf{d}_k = \delta_k \frac{\mathbf{d}_{k-1}}{\|\mathbf{d}_{k-1}\|} + (1 - \delta_k) \frac{\nabla f(\mathbf{y}_k)}{\|\nabla f(\mathbf{y}_k)\|}, \quad (33)$$

summarized in Alg. 7. In Sec. IV, we experimentally prove this heuristic to significantly reduce the number of steps for distance computations for non-strictly convex shapes. We also show that this heuristic does not need to be applied to the Polyak acceleration, as, contrary to the Nesterov acceleration, the Polyak acceleration does not compute an intermediary point \mathbf{y}_k .

IV. EXPERIMENTS

In this section, we study the performance of both Polyak and Nesterov-accelerated GJK (Alg. 6) against the vanilla GJK (Alg. 4) algorithm.

In sections IV-A and IV-B, we benchmark our proposed Polyak-accelerated and Nesterov-accelerated GJK algorithms against the vanilla GJK algorithm on these two distinct benchmarks. The benchmark made of strictly-convex shapes represents a worst-case scenario regarding the number of iterations for all variants of GJK. The benchmark of non-strictly convex shapes represents shapes typically used in robotic or computer graphics applications. In Sec. IV-C, we benchmark GJK and our proposed accelerated gradients against the state-of-the-art quadratic programming solver ProxQP [50]. We show that GJK and our proposed accelerated variants vastly outperform generic quadratic programming (QP) solvers, making these QP solvers prohibitive for collision detection. Then, in Sec. IV-D, we compare our methods and our implementation of vanilla GJK against different collision detection solvers of various collision detection libraries. Finally, in Sec. IV-E, we benchmark vanilla, Polyak-accelerated, and Nesterov-accelerated GJK on a dataset of trajectories obtained using a physics simulator. We show that, similarly to vanilla GJK, our accelerated GJK algorithms can benefit from being warm-started with previous simulation time steps, outperforming the vanilla GJK in physics simulation scenarios.

Implementation. We leverage the HPP-FCL C++ library [28], [51], an extension of the original FCL library [28]. Unlike FCL, HPP-FCL provides its own implementation of GJK, which we have extended by implementing the Polyak and Nesterov-accelerated GJK algorithms (Alg. 6). The open-source code of the HPP-FCL library is publicly available at <https://github.com/humanoid-path-planner/hpp-fcl> under the BSD-3 license. The benchmark code is publicly available at <https://github.com/lmontaut/colbench> under the GNU AGP License.

Shapes datasets. To distinguish between pairs of strictly convex and non-strictly convex shapes, we build a first benchmark only composed of pairs of ellipsoids (strictly convex shapes) and a second benchmark using pairs of standard meshes (represented by their convex hulls) which are taken from the commonly-used YCB dataset [52].

Ellipsoids. In the ellipsoids benchmark, the ellipsoids are randomly generated by sampling positive-definite matrices. In total, we generate 1000 random pairs of ellipsoids. Given a pair of ellipsoids, we randomly sample relative poses between the shapes, using a uniform distribution for the relative rotation between the shapes. Regarding the translation part of the random poses, the directions are selected at random, but the norms are chosen so that we control the distance $\text{dist}(\mathcal{A}_1, \mathcal{A}_2)$ between the objects. This enables us to measure the influence of the separation distance on the performance of the studied algorithms. The values used for $\text{dist}(\mathcal{A}_1, \mathcal{A}_2)$ range from -0.1 m to 1 m. Negative values correspond to scenarios where the shapes intersect, with $\text{dist}(\mathcal{A}_1, \mathcal{A}_2)$ corresponding to the separating vector's norm. The separating vector is the vector of the smallest norm needed to translate one of the two shapes such that the two shapes do not intersect. Therefore, for each pair of ellipsoids, 100 random relative poses are sampled, so the shapes do not intersect. We translate the shapes along the axis given by their closest points for each relative pose to

study the impact of $\text{dist}(\mathcal{A}_1, \mathcal{A}_2)$. We then set $\text{dist}(\mathcal{A}_1, \mathcal{A}_2)$ to fixed values between -0.1 m to 1 m.

YCB meshes. On the other hand, the YCB mesh dataset contains about 60 shapes commonly used for robotic manipulation tasks (kitchen appliances, tools, toys, etc.). Each object has three different resolution levels corresponding to the number of points representing the mesh. For each object, we take the lowest resolution, i.e., the *google-16k* versions of the meshes, as it is resolute enough for any robotic task. As GJK-like algorithms work on convex shapes, we pre-compute the convex hulls of each object in the YCB dataset. This procedure needs only to be done once; if more precision is required for a certain robotic task, it is common to decompose a non-convex object into a set of convex sub-objects. For the sake of simplicity, we will not decompose YCB objects into sub-objects, as the results presented in this section would essentially be the same. In the rest of this section, when we mention a shape, we refer to its convex hull unless explicitly stated otherwise. The resulting meshes extracted from the YCB dataset contain between 100 and 8000 vertices. About 50% of meshes contain between 100 and 1000 vertices. As in the ellipsoids benchmark, 100 random relative poses are sampled for each pair such that the shapes do not intersect and then set $\text{dist}(\mathcal{A}_1, \mathcal{A}_2)$ to fixed values between -0.1 m and 1 m.

In both benchmarks (ellipsoids and YCB meshes), the characteristic sizes of the shapes range from a few centimeters up to a meter. Finally, for the distance computation problem, we select a convergence tolerance of $\epsilon = 10^{-8}$.

Initialization strategy. Apart from Sec. IV-E, the GJK algorithm and our proposed accelerated GJK algorithms are initialized with the centers of the shapes' bounding boxes. The bounding box of a shape fully encapsulates it, as is shown in Fig. 1. Hence, if we denote c_1 and c_2 the geometric centers of the bounding boxes of \mathcal{A}_1 and \mathcal{A}_2 , then we initialize vanilla GJK, Polyak-accelerated GJK and Nesterov-accelerated GJK to $x_0 = c_1 - c_2$.

Metrics. To measure the performances of Polyak-accelerated GJK, Nesterov-accelerated GJK, and the vanilla GJK algorithms, we measure the number of iterations N^k to solve a given collision problem. For the mesh benchmark, we also measure the execution time T^μ of both methods. We solve each generated collision problem 100 times to cope with CPU throttling. We then report the average of the 90% lowest computation times. All the benchmarks in this paper were run on an Apple M1 Max CPU.

A. Worst case scenario: strictly convex shapes - ellipsoids

We first focus on the ellipsoid benchmark to get a statistical understanding of the performance of Polyak and Nesterov-accelerated GJK against vanilla GJK. In the following, we explain why these shapes are interesting to study experimentally, as they represent the worst-case scenario that GJK-like algorithms can be confronted with. First, as previously explained, GJK-like algorithms look for the optimal active set of the solution x^* . Otherwise said, GJK-like methods find a set of support points $W^* = \{s^1, s^2, \dots\}$ such that the optimal solution x^* is a convex combination of the points

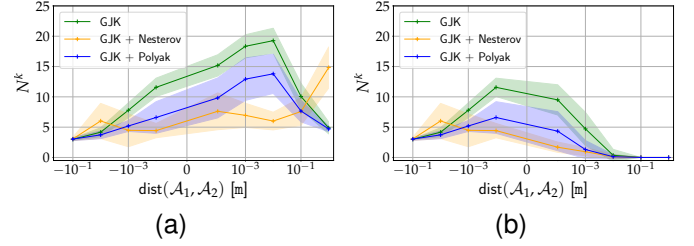


Fig. 7. Comparison of Polyak-accelerated GJK, Nesterov-accelerated GJK, and vanilla GJK on the ellipsoid benchmark for (a) distance computation and (b) Boolean collision checking. The graphs show the number of iterations (y-axis) vs. the signed distance between the two shapes (x-axis). The curve shows the mean value over 100,000 random trials. The shaded region corresponds to the standard deviation. The Nesterov-accelerated GJK algorithm requires fewer iterations when the shapes are in close proximity. The Polyak-accelerated GJK algorithm is more robust when shapes are strongly overlapping or distant.

of W^* , where s^i are support points computed while running GJK or our proposed accelerations. Then, contrary to non strictly-convex shapes, strictly-convex shapes have an infinite amount of support points. As explained at the end of Sec. III, each normalized support direction d corresponds to a unique support point $S_{\mathcal{D}}(d)$. Therefore, it is fundamentally harder to identify the optimal active set when considering strictly-convex shapes, as there is an infinite amount of potential support points to consider. In contrast, there is a finite amount of support points to consider when using non strictly-convex shapes.

In Fig. 7, we show the performance of the vanilla, the Polyak-accelerated, and the Nesterov-accelerated GJK algorithms on the ellipsoids benchmark. Fig. 7a and Fig. 7b show the mean and standard deviation of the number of iterations N^k of each method for the distance computation and the Boolean collision checking problems, respectively. When the shapes are shallowly intersecting, Polyak and Nesterov-accelerated GJK converge with the same or even fewer number of iterations than vanilla GJK. However, the shallower the penetration, the more Polyak and Nesterov accelerate over vanilla GJK, with Nesterov providing the most acceleration. The irregularity in standard deviation at -0.01 m is a critical zone for the Nesterov momentum where the variance increases. When shapes are in close proximity, the Nesterov acceleration of GJK significantly reduces the number of iterations compared to vanilla GJK and Polyak-accelerated GJK. Finally, when shapes are distant, $1 \text{ m} \leq \text{dist}(\mathcal{A}_1, \mathcal{A}_2)$, the Nesterov acceleration is detrimental to convergence on the distance computation problem while Polyak-accelerated GJK remains competitive against vanilla GJK. This indicates that the Polyak acceleration is generally more robust than the Nesterov acceleration. However, it offers less acceleration over vanilla GJK when the shapes are in close-proximity or shallowly overlapping. A similar pattern of speed-ups of Polyak and Nesterov-accelerated GJK over vanilla GJK is shown for the collision detection problem in Fig. 7b.

B. Non-strictly convex shapes: meshes

Effect of support direction normalization. For meshes, the importance of normalizing the support direction (see Eq. (33))

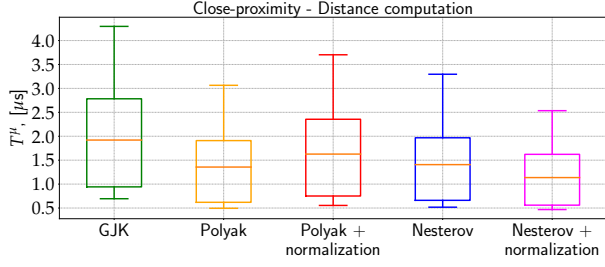
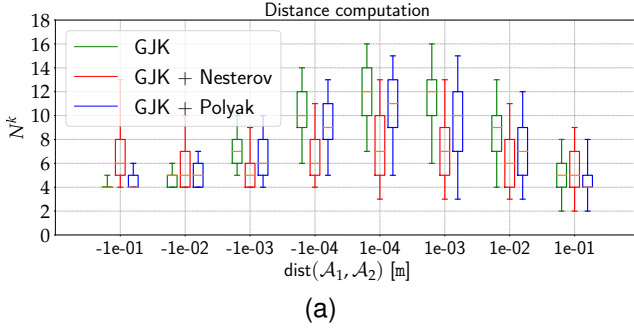
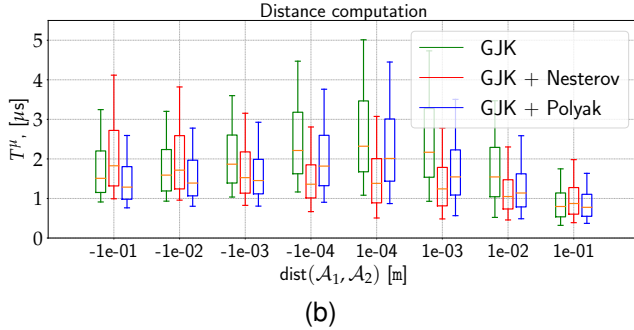


Fig. 8. Impact of support direction normalization in Polyak and Nesterov-accelerated GJK on the YCB benchmark. The graph shows the computation time T^μ (lower is better) for vanilla GJK, Polyak-accelerated GJK, and Nesterov-accelerated GJK with and without support direction normalization. Here, the two shapes are in close-proximity: $0 \text{ m} < \text{dist}(\mathcal{A}_1, \mathcal{A}_2) \leq 0.1 \text{ m}$. Normalizing the support direction benefits Nesterov-accelerated GJK, reducing the overall number of iterations compared to GJK and non-normalized Nesterov-accelerated GJK.



(a)

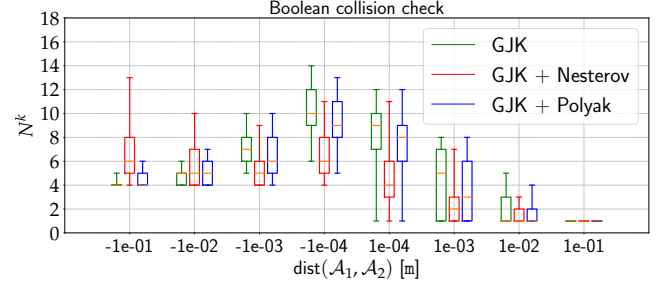


(b)

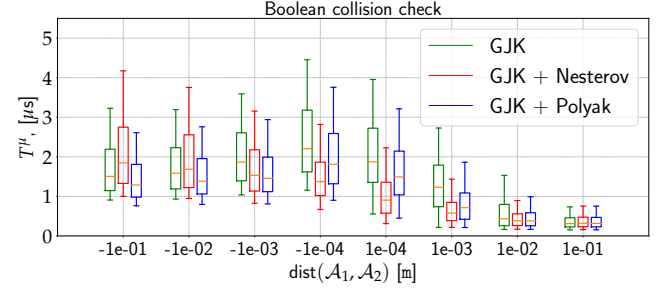
Fig. 9. Distance computation on the YCB benchmark. The graphs show the number of iterations N^k (a) and the execution time T^μ (b) for Polyak-accelerated GJK, Nesterov-accelerated GJK (with normalization) and vanilla GJK for a range of distances (x-axis) between the shapes. For both metrics, lower is better.

in the Nesterov-accelerated GJK is highlighted in Fig. 8. For both the distance computation and Boolean collision checking problems, the normalization heuristic prevents the Nesterov acceleration from reaching a fixed point too early, and consequently, it reduces the overall amount of iterations needed to converge. This is, however, not the case for the Polyak-accelerated GJK algorithm, which does not benefit from support normalization. As explained at the end of Sec. III, the Polyak acceleration does not compute an intermediary point, unlike the Nesterov acceleration scheme. In the following, we thus focus only on Polyak-accelerated GJK *without* support normalization and Nesterov-accelerated GJK *with* support normalization. We compare the performances of these two algorithms against the vanilla GJK algorithm.

Statistical validation over the YCB dataset. In Fig. 9 and Fig. 10, we report the number of iterations N^k and execution

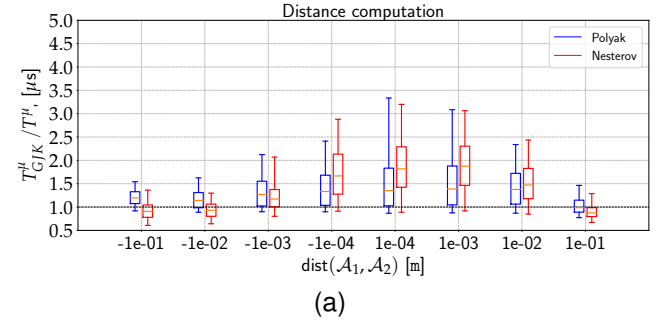


(a)

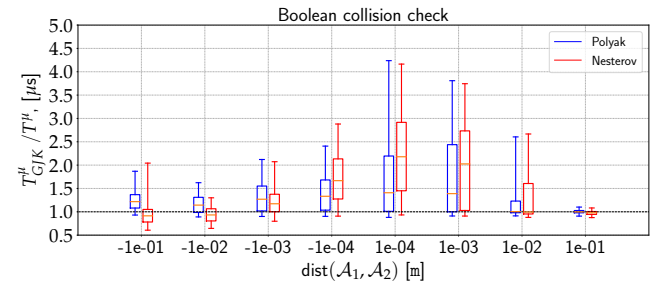


(b)

Fig. 10. Boolean collision check on the YCB benchmark. The graphs show the number of iterations N^k (a) and the execution time T^μ (b) for the Polyak-accelerated GJK, Nesterov-accelerated GJK (with normalization), and vanilla GJK algorithms for a range of distances (x-axis) between the shapes. For both metrics, lower is better.



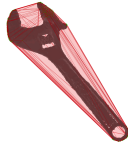
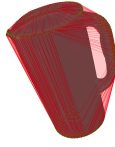
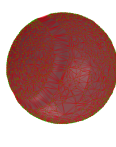



(a)



(b)

Fig. 11. Speed-ups of Polyak and Nesterov-accelerated GJK over vanilla GJK on the YCB benchmark. The plots show ratios of the number of execution times for (a) distance computation and (b) boolean collision checking of Polyak-accelerated GJK and Nesterov-accelerated GJK (with normalization) against vanilla GJK. Ratios over 1.0 show speed-ups of accelerated GJK over vanilla GJK. For both metrics, higher is better.

TABLE I
COMPUTATION TIMES (μs) FOR DISTANCE COMPUTATION (T_D^μ) AND BOOLEAN COLLISION CHECKING (T_C^μ) ON THE YCB BENCHMARK FOR CLOSE-PROXIMITY OR SHALLOWLY INTERSECTING SHAPES. n DENOTES THE NUMBER OF VERTICES FOR EACH MESH.

$N = 240$					$N = 1811$			$N = 3585$			
											
	GJK	Polyak	Nesterov		GJK	Polyak	Nesterov		GJK	Polyak	Nesterov
	T_D^μ	1.1 ± 0.3	0.9 ± 0.3	0.9 ± 0.3	1.9 ± 0.5	1.5 ± 0.5	1.4 ± 0.5	3.2 ± 0.8	2.3 ± 0.7	2.4 ± 0.7	
	T_C^μ	0.9 ± 0.4	0.7 ± 0.4	0.8 ± 0.4	1.5 ± 0.6	1.2 ± 0.6	1.1 ± 0.6	2.5 ± 0.9	1.7 ± 0.8	1.9 ± 1.0	
	T_D^μ				2.7 ± 0.8	2.1 ± 0.7	1.9 ± 0.6	4.0 ± 1.0	2.9 ± 0.9	2.9 ± 1.0	
	T_C^μ				2.3 ± 0.8	1.6 ± 0.8	1.5 ± 0.8	3.1 ± 1.2	2.1 ± 1.0	2.2 ± 1.3	
	T_D^μ							4.4 ± 1.3	2.9 ± 1.0	3.0 ± 0.9	
	T_C^μ							3.0 ± 1.9	2.1 ± 1.4	2.1 ± 1.4	

time T^μ for Polyak-accelerated GJK, Nesterov-accelerated GJK and vanilla GJK. In Fig. 11, we report relative accelerations $T_{GJK}^\mu / T_{polyak}^\mu$ and $T_{GJK}^\mu / T_{Nesterov}^\mu$ of Polyak-accelerated compared to GJK. These relative accelerations are computed on a given collision problem, and Fig. 11 reports their statistical distributions. These relative measures allow analyzing the effects of the studied algorithms on the same collision problems, which are not captured when using absolute values. Overall, Polyak and Nesterov-accelerated GJK significantly reduce the execution time when compared to GJK in cases where shapes are shallowly intersecting or in close-proximity. It is worth recalling, at this stage, that when two shapes are relatively far from each other, any broadphase algorithm will automatically discard such a pair. Only in a small percentage of cases, Polyak-accelerated GJK and Nesterov-accelerated GJK are slower than GJK. When measuring the absolute performance of the two proposed methods, Polyak-accelerated GJK provides less acceleration than Nesterov-accelerated GJK in critical cases with close proximity and shallowly overlapping collision problems. However, Polyak-accelerated GJK is more robust than Nesterov-accelerated GJK as it is almost always better than vanilla GJK, even when the shapes are distant or overlap.

In Table. I, we select three meshes with an increasing number of vertices to highlight the benefits of the Polyak and Nesterov accelerations. For each pair, we report the mean and the standard deviation of the execution time for distance computation and Boolean collision checking. We consider the challenging set-up of close-by or shallowly intersecting shapes in the range of separation distances $-0.01 \text{ m} \leq \text{dist}(\mathcal{A}_1, \mathcal{A}_2) \leq 0.01 \text{ m}$. The lower mean and standard deviation show that Polyak and Nesterov-accelerated GJK are faster than the vanilla GJK and reduce the spread of computation times across the different collision problems in

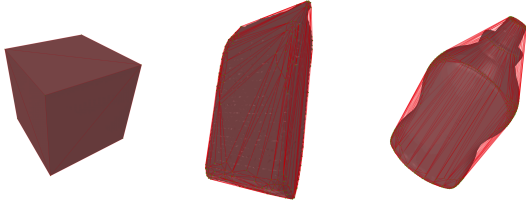
this setting.

From this benchmark involving shapes from the YCB dataset, we can distinguish two use cases in which one would prefer using Polyak-accelerated GJK compared to Nesterov-accelerated and vice-versa. In tasks where the exact distance between the shapes needs to be computed and where this distance separating the shapes can take any value, due to its robustness, the Polyak-accelerated GJK algorithm is better suited than its Nesterov counterpart. However, in a situation involving shapes interacting at close proximity, like in a contact physics simulation, it is preferable to choose the Nesterov-accelerated GJK. Before studying the performance of GJK and our proposed accelerations for physics simulation, we first show the benefits of using GJK-based algorithms for collision detection instead of standard off-the-shelf optimization solvers and provide a comparison of the implementations of our methods against baselines from other collision detection libraries.

C. GJK-like algorithms vs. generic quadratic programming solvers

As explained in Sec. II, in the case of two convex meshes, the collision problem can be formulated as a Quadratic Program (2) (QP), which can be solved using any generic QP solver [50], [53]–[56]. In Table II, we compare the performance of GJK and our proposed accelerations against the state-of-the-art ProxQP solver [50]. We report the computation timings in micro-seconds for pairs of identical shapes with an increasing number of vertices (N_v) and faces (N_f). The results are staggering: for very simple convex meshes like a cube, GJK, and its accelerated variants are already more than 10 times faster than the QP solver. When the complexity of the meshes increases, GJK and its variants are thousands to tens of thousands of times faster than the QP solver, making

TABLE II
COMPUTATION TIME IN MICRO-SECONDS OF GJK-LIKE SOLVERS VS.
SOTA QUADRATIC PROGRAMMING PROXQP SOLVER.



	$N_v = 8$ $N_f = 6$	$N_v = 250$ $N_f = 496$	$N_v = 940$ $N_f = 1876$
ProxQP	$5.3 \pm 2.7 \mu s$	$(2 \pm 0.6) \cdot 10^3 \mu s$	$(20 \pm 14) \cdot 10^3 \mu s$
GJK	$0.2 \pm 0.03 \mu s$	$0.8 \pm 0.3 \mu s$	$2.1 \pm 0.5 \mu s$
Nesterov	$0.2 \pm 0.05 \mu s$	$0.7 \pm 0.2 \mu s$	$1.4 \pm 0.3 \mu s$
Polyak	$0.2 \pm 0.05 \mu s$	$0.6 \pm 0.2 \mu s$	$1.4 \pm 0.4 \mu s$

generic QP solvers prohibitive for collision detection in real-time applications like robotics or computer graphics. Although these results are not surprising, they clearly showcase why dedicated solvers such as GJK-like methods are crucial for collision detection.

D. Comparison against other collision detection libraries

In this sub-section, we compare our implementations of vanilla, Nesterov-accelerated and Polyak-accelerated GJK against the following baselines from other collision detection libraries: CCD's MPR and GJK implementations [15], FCL's GJK implementation [16] and Bullet's GJK implementation. These collision detection algorithms are used in physics simulators like Drake [18], MuJoCo [3], ODE [19] and Bullet [1]. Since GJK is the state-of-the-art algorithm for narrow phase collision detection, it is no surprise that most collision detection libraries implement only this algorithm. In addition to being a general, robust and computationally fast method, GJK-like algorithms also have the advantage of producing a simplex surrounding the origin when shapes are in collision (see Sec. II). This simplex is then fed to the Expanding Polytope Algorithm (EPA) in order to estimate the penetration depth and separation vector [22]; these contact informations are used in physics simulation to resolve contact constraints. Just like GJK, the core of EPA consist in computing support points in order to expand a polytope inside the Minkowski difference. Therefore, since GJK and EPA are made to work in succession with one another, it is almost always the case that physics simulators use GJK to first detect collisions and then EPA to compute contact features if a collision is detected. All the libraries listed before are written either in C or in C++.

In Fig. 12, we report the performance of the methods listed before on the YCB benchmark used in Sec. IV-B. We measure the execution time of the different collision detection solvers on the boolean collision check task and divide the results into three distance categories: when shapes are distant ($\text{dist}(\mathcal{A}_1, \mathcal{A}_2) \geq 1\text{m}$), when shapes are in close-proximity ($0\text{m} \leq \text{dist}(\mathcal{A}_1, \mathcal{A}_2) \leq 0.1\text{m}$) and when shapes are overlapping ($\text{dist}(\mathcal{A}_1, \mathcal{A}_2) \leq 0\text{m}$). The collision problems corresponding to the *distant* case would typically be filtered by the broadphase. We report them to give a clear picture of the performance of the different implementations. In practice,

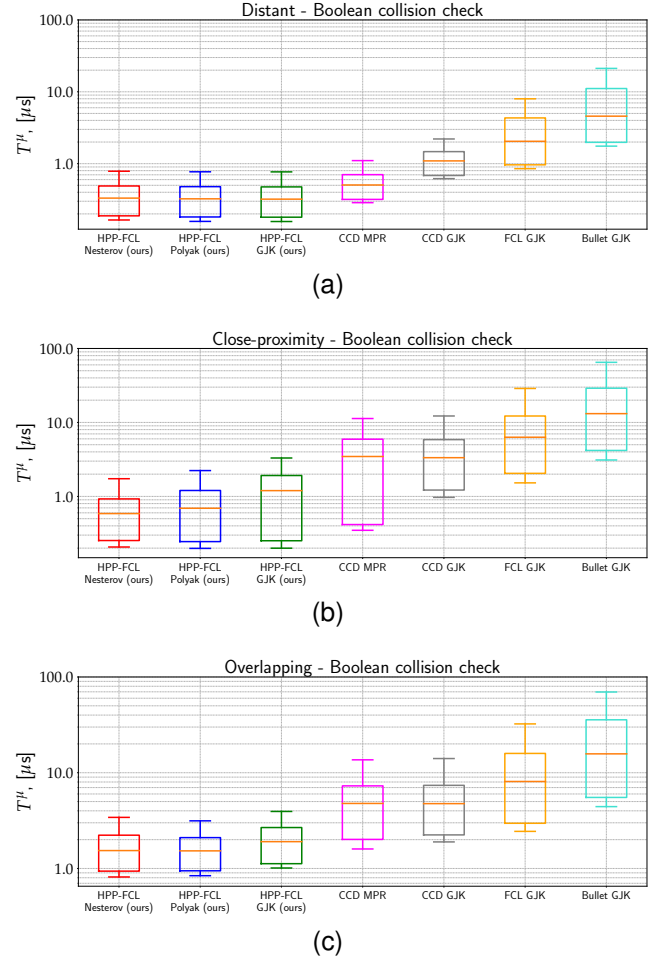


Fig. 12. Computation time in micro-seconds of implementations of different collision detection solvers from various C/C++ libraries on the YCB benchmark for boolean collision checking. The y-axis is a log-scale. We compare our implementation of vanilla GJK, Nesterov-accelerated GJK and Polyak-accelerated GJK against FCL's GJK implementation, CCD's GJK implementation and CCD's MPR implementation. The results are split into three different categories: (a) when shapes are distant ($\text{dist}(\mathcal{A}_1, \mathcal{A}_2) \geq 1\text{m}$), (b) in close-proximity ($0 \leq \text{dist}(\mathcal{A}_1, \mathcal{A}_2) \leq 0.1\text{m}$) and (c) overlapping ($\text{dist}(\mathcal{A}_1, \mathcal{A}_2) \leq 0\text{m}$). Lower is better.

the *close-proximity* and *overlapping* cases correspond to situations when the different collision detection solvers are actually called; the broad phase cannot filter such collision problems and the narrow phase is then called.

The results show our implementation of GJK and our proposed methods outperform the solvers of the other collision detection libraries. We find similar results for the distance computation task. We now turn our attention to the context of physics simulation and show that our proposed methods, just like GJK, can be warm-started by using previous simulation steps.

E. Collision detection for physics simulation

In the previous benchmarks, we have experimentally shown the improvement of our methods, Polyak-accelerated GJK and Nesterov-accelerated GJK, over the vanilla GJK algorithm for collision problems which are important in practice, *i.e.* when the broadphase has not filtered collision pairs and are thus overlapping or in close proximity. So far, the benchmarks

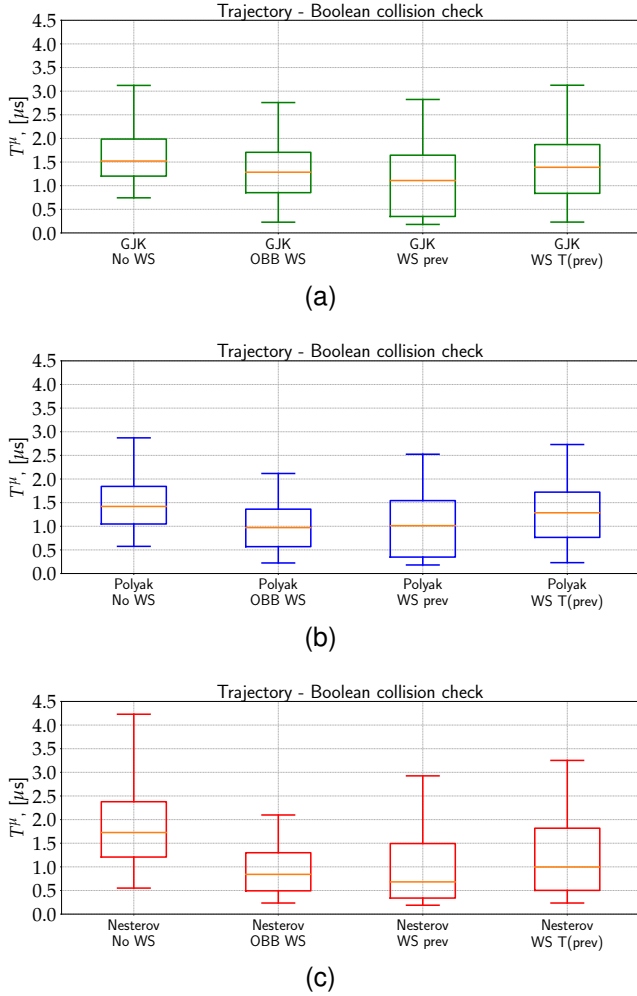


Fig. 13. Boolean collision checking of YCB objects' trajectories (see Fig. 14) for different warm-start strategies for (a) vanilla GJK, (b) Polyak-accelerated GJK, and (c) Nesterov-accelerated GJK (with normalization). In the three figures, WS is an abbreviation of *warm-start*. The *No WS* strategy signifies the algorithm is initialized with $\mathbf{x}_0 = (1, 0, 0)^T$. The *OBB WS* strategy uses the objects' current OBBs centers to compute \mathbf{x}_0 . In both *WS prev* and *WS T(prev)*, \mathbf{x}_0 is computed using GJK or EPA's previous solution, when this solution is available (i.e., when the previous collision problem was not discarded by the broadphase). Contrary to *WS prev*, *WS T(prev)* corrects the previous solution using the relative displacement of the shapes between the two considered time steps.

have been constructed by randomly selecting poses for our shapes. However, in robotics applications such as trajectory optimization, motion planning, or computer graphics, the successive poses between objects are usually correlated by time. In this sub-section, we study how vanilla GJK, Polyak-accelerated GJK, and Nesterov-accelerated GJK can be warm-started using the previous time instant, as occurring inside physics simulators.

To do so, we create a dataset of trajectories using pairs of objects from the YCB dataset used in Sec. IV-B. We randomly select 1000 pairs of YCB objects and drop them in a funnel as shown in Fig. 14. At the beginning of the simulation, each object is given a random pose and random translational and rotational velocities. The simulation is then run at 120Hz for 1 second. When a collision occurs, the GJK and EPA (expanding polytope algorithm) algorithms are called to determine the position of the contact points and the corresponding normal

for the considered pair of objects. The collision is then resolved using a contact solver based on the Projected Gauss-Seidel [57] algorithm to account for a second-order cone representing friction, following the implementation proposed in [58]. In total, 120k collision problems are generated. For each collision problem, we extract the YCB shapes and their poses.

This dataset allows us to evaluate the vanilla, Polyak-accelerated, and Nesterov-accelerated GJK algorithms on the same collision problems generated by a physics simulation. Interestingly, this dataset allows us to study only the collision problems not filtered by the broadphase of the physics simulator, as explained in Sec. I. During the broad phase, the oriented bounding boxes of the objects (OBBs, as shown in Fig. 1) are used to assess if objects are not in collision. Therefore, if the broad phase does not filter a collision, the GJK algorithm and our proposed accelerations are called and solve the boolean collision check problem. Finally, this dataset allows us to test different strategies to warm-start (WS) the GJK algorithm and our proposed accelerations. We denote by \mathbf{x}_0^t the initial guess given to vanilla, Polyak-accelerated and Nesterov-accelerated GJK at time step t of the simulation. We also denote by \mathbf{x}^{t-1} the separation vector found by GJK (accelerated or not) or EPA at time-step $t - 1$ of the simulation. We consider four different warm-start strategies for the vanilla GJK algorithm and our proposed accelerations:

- 1) the first strategy is the *No WS* strategy, where the vanilla, Polyak, and Nesterov GJK algorithms are initialized using $\mathbf{x}_0^t = (1, 0, 0)^T$. This strategy serves as a baseline for the other warm-start strategies.
- 2) The second strategy is the *OBB WS* strategy, where $\mathbf{x}_0^t = \mathbf{c}_1^t - \mathbf{c}_2^t$ with \mathbf{c}_1^t and \mathbf{c}_2^t being the centers of the considered objects' oriented bounding boxes. This warm-start is used in all the previous benchmarks, as explained at the beginning of this section.
- 3) The third strategy is the *WS prev* strategy, where $\mathbf{x}_0 = \mathbf{x}^{t-1}$ is initialized using the solution found by GJK or EPA in the previous simulation time step.
- 4) The fourth and last strategy is the *WS T(prev)* strategy. The difference with the *WS prev* strategy is that we use the relative transformation of the shapes between time steps t and $t - 1$ to anticipate how \mathbf{x}^{t-1} might move between these two time steps.

The last two warm-starting strategies might not always be actionable. Indeed, if at time step $t - 1$ the broad phase finds no collision between the two considered shapes, the GJK and EPA algorithms are not called, and therefore, \mathbf{x}^{t-1} does not exist. Consequently, if GJK needs to be called at time step t , it cannot use \mathbf{x}^{t-1} . In such a case, these two strategies fall back to the second strategy, which exploits the objects' OBBs.

We run vanilla, Polyak-accelerated and Nesterov-accelerated GJK on the dataset of trajectories described previously; the results of this benchmark are summed up in Fig. 13. In this figure, we report the computation time of the boolean collision check for GJK and our proposed accelerations. Importantly, this figure only considers the collision problems *which were not filtered by the broad*

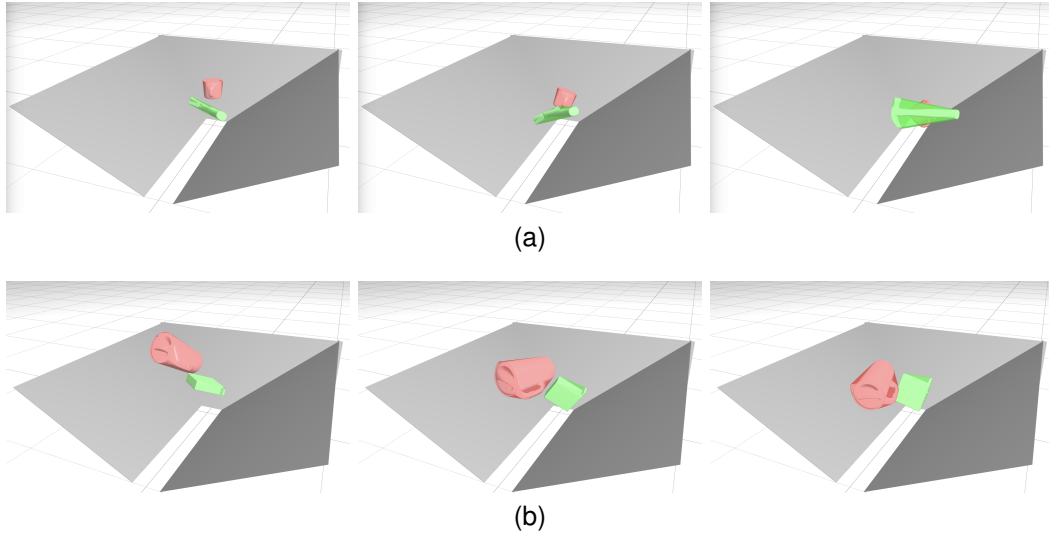


Fig. 14. Two different trajectories (a) and (b) with two different pairs of objects from the YCB dataset. The objects are dropped with a random initial velocity for each trajectory in a funnel (the grey walls). At each time step, if the broadphase cannot discriminate if the shapes are in collision or not, we use the vanilla GJK algorithm or our proposed Polyak and Nesterov-accelerated variants of GJK to determine if a collision occurs between the convex-hulls of the collision pair.

phase, as GJK or its accelerations would not be called otherwise. In doing so, we aim to provide the clearest possible picture of the computation time dedicated to GJK in a physics computation. Due to the filtering of the broad phase, the typical distance separating the shapes is less than a few centimeters; this corresponds to the overlapping and close-proximity cases described in the previous benchmarks. First, the results show that for the three studied methods, the *No WS* and *WS $T(\text{prev})$* warm-start strategies provided a worse initial guess than the two other warm-start strategies. It appears that the *WS $T(\text{prev})$* strategy is often the worse strategy; this observation means that the separation vector computed by GJK and/or EPA moves in a non-trivial manner between time steps $t - 1$ and t of the simulation. For vanilla GJK, the best warm-starting strategy is the *WS prev* strategy, which re-uses the separation vector computed by GJK and EPA at time step $t - 1$ of the simulation. For Polyak-accelerated GJK, both the *OBBS WS* and *WS prev* strategies perform better than vanilla GJK's best warm-starting strategy. However, contrary to GJK, the *OBBS WS* strategy is arguably better than the *WS prev* strategy as it greatly reduces the variance of the computation timings distribution. For Nesterov-accelerated GJK, the results are even more significant: both the *OBBS WS* and *WS prev* strategy significantly outperform GJK with its best warm-starting strategy. When using the *OBBS WS* and *WS prev* strategies, the Nesterov acceleration allows the median of computation times to reach close to $0.5\mu\text{s}$, compared to a median above $1\mu\text{s}$ in the case of GJK's best warm-starting strategy. Like the Polyak acceleration, the Nesterov-accelerated GJK algorithm significantly reduces the spread of the distribution of computation times compared to GJK. This is especially visible when using the *OBBS WS* strategy together with the Nesterov acceleration. Finally, this benchmark shows that physics simulation strongly benefits from using Nesterov-accelerated GJK warm-started using the *OBBS WS* strategy.

V. CONCLUSION

In this work, we have first established that the well-known GJK algorithm can be understood as a variant of the Frank-Wolfe method, well studied within the convex optimization community, and more precisely, GJK can be identified as a sub-case of fully-corrective Frank-Wolfe. Subsequently, this connection has enabled us to accelerate the GJK algorithm in the sense of Nesterov acceleration by adapting recent contributions on applying Polyak and Nesterov acceleration to the context of Frank-Wolfe. Through extensive benchmarks, we have shown that this acceleration is beneficial for both collision detection and distance computation settings for scenarios where shapes intersect or are close, accelerating collision detection by up to a factor of two. Interestingly, these two scenarios notably encompass the generic contexts of planning and control as well as physical simulation, which are essential areas of modern robotics. Therefore, although the proposed accelerations correspond to improvements of GJK's execution time on the order of a few microseconds, modern robotics applications may solve millions to billions of collision problems when, for instance, learning a policy with RL [59].

The Polyak and Nesterov accelerations for GJK are already included in the HPP-FCL library [51], notably used by the HPP framework [4] for motion planning, the Pinocchio framework [60] dedicated to simulation and modeling, the Crocodyl [61] and the OSC-2 [62] software dedicated to trajectory optimization, to name a few. In future work, we plan to leverage these accelerated collision detection algorithms in the scope of differentiable collision detection [63], differentiable simulation [64], [65] and constrained optimal control involving contact interactions [61], [66], [67].

Finally, one can expect this work to be largely adopted in the current available GJK implementations, as it only requires minor algorithmic changes. This work should benefit a large audience within robotics (e.g., simulation, planning, control) and beyond by addressing issues shared by other communities, including computer graphics and computational geometry.

ACKNOWLEDGMENTS

We warmly thank Francis Bach, Adrien Escande, Joseph Mirabel, and Mehdi Bennaïgue for fruitful discussions on the various topics covered by this article. We also warmly thank the cohort of developers who contribute to developing open-source, useful, reproducible, and extensible software, which primarily benefits this project and, more widely, the robotics ecosystem.

This work was partly supported by the European Regional Development Fund under the project IMPACT (reg. no. CZ.02.1.01/0.0/0.0/15 003/0000468), by the French government under the management of Agence Nationale de la Recherche as part of the “Investissements d’avenir” program, reference ANR-19-P3IA-0001 (PRAIRIE 3IA Institute), through the project INEXACT (ANR-22-CE33-0007-01), by the AGIMUS project, funded by the European Union under GA no.101070165, by the ERC project FRONTIER (no. 101097822) - views and opinions expressed are those of the author(s) only and do not necessarily reflect those of the European Union or the European Commission, neither the European Union nor the European Commission can be held responsible for them - and by the Louis Vuitton ENS Chair on Artificial Intelligence.

REFERENCES

- [1] E. Coumans and Y. Bai, “Pybullet, a python module for physics simulation for games, robotics and machine learning,” 2016.
- [2] Nvidia, “Persistent contact manifold,” 2008.
- [3] E. Todorov, T. Erez, and Y. Tassa, “Mujoco: A physics engine for model-based control,” in *2012 IEEE/RSJ international conference on intelligent robots and systems*. IEEE, 2012, pp. 5026–5033.
- [4] J. Mirabel, S. Tonneau, P. Fernbach, A.-K. Seppälä, M. Campana, N. Mansard, and F. Lamirault, “Hpp: A new software for constrained motion planning,” in *2016 IEEE/RSJ International Conference on Intelligent Robots and Systems (IROS)*. IEEE, 2016, pp. 383–389.
- [5] M. A. Toussaint, K. R. Allen, K. A. Smith, and J. B. Tenenbaum, “Differentiable physics and stable modes for tool-use and manipulation planning,” *Robotics: Science and Systems*, 2018.
- [6] J. Schulman, Y. Duan, J. Ho, A. Lee, I. Awwal, H. Bradlow, J. Pan, S. Patil, K. Goldberg, and P. Abbeel, “Motion planning with sequential convex optimization and convex collision checking,” *The International Journal of Robotics Research*, vol. 33, no. 9, pp. 1251–1270, 2014.
- [7] C. Ericson, *Real-time collision detection*. Crc Press, 2004.
- [8] K. Mamou and F. Ghorbel, “A simple and efficient approach for 3d mesh approximate convex decomposition,” in *2009 16th IEEE international conference on image processing (ICIP)*. IEEE, 2009, pp. 3501–3504.
- [9] E. Gilbert and D. Johnson, “Distance functions and their application to robot path planning in the presence of obstacles,” *IEEE Journal on Robotics and Automation*, vol. 1, no. 1, pp. 21–30, 1985.
- [10] O. Stasse, A. Escande, N. Mansard, S. Miossec, P. Evrard, and A. Kheddar, “Real-time (self)-collision avoidance task on a hrp-2 humanoid robot,” in *2008 IEEE international conference on robotics and automation*. IEEE, 2008, pp. 3200–3205.
- [11] M. Frank and P. Wolfe, “An algorithm for quadratic programming,” *Naval research logistics quarterly*, vol. 3, no. 1-2, pp. 95–110, 1956.
- [12] E. G. Gilbert, D. W. Johnson, and S. S. Keerthi, “A fast procedure for computing the distance between complex objects in three-dimensional space,” *IEEE Journal on Robotics and Automation*, vol. 4, no. 2, pp. 193–203, 1988.
- [13] B. Li, A. Sadeghi, and G. Giannakis, “Heavy ball momentum for conditional gradient,” *Advances in Neural Information Processing Systems*, vol. 34, pp. 21 244–21 255, 2021.
- [14] B. Li, M. Coutino, G. B. Giannakis, and G. Leus, “A momentum-guided frank-wolfe algorithm,” *IEEE Transactions on Signal Processing*, vol. 69, pp. 3597–3611, 2021.
- [15] D. Fiser, “Github: libccd,” <https://github.com/danfis/libccd>, 2010.
- [16] J. Pan, S. Chitta, and D. Manocha, “Github: Fcl – the flexible collision library,” 2012.
- [17] E. Coumans, “Github: Bullet physics sdk,” <https://github.com/bulletphysics/bullet3>, 2015.
- [18] R. Tedrake and the Drake Development Team, “Drake: Model-based design and verification for robotics,” 2019. [Online]. Available: <https://drake.mit.edu>
- [19] R. L. Smith, “Github: The open dynamics engine (ODE),” <https://github.com/thomasmarsh/ODE>, 2001–2007.
- [20] L. Montaut, Q. Lidec, V. Petrík, J. Sivic, and J. Carpentier, “Collision Detection Accelerated: An Optimization Perspective,” in *Proceedings of Robotics: Science and Systems*, New York City, NY, USA, June 2022.
- [21] G. v. d. Bergen, “A fast and robust gjk implementation for collision detection of convex objects,” *Journal of graphics tools*, vol. 4, no. 2, pp. 7–25, 1999.
- [22] G. Van den Bergen, “Proximity Queries and Penetration Depth Computation on 3D Game Objects,” in *Game Developers Conference*, 2001.
- [23] M. C. Lin and J. F. Canny, “A fast algorithm for incremental distance calculation,” in *ICRA*, vol. 91, 1991, pp. 9–12.
- [24] B. Mirtich, “V-clip: Fast and robust polyhedral collision detection,” *ACM Transactions On Graphics (TOG)*, vol. 17, no. 3, pp. 177–208, 1998.
- [25] S. Cameron, “A comparison of two fast algorithms for computing the distance between convex polyhedra,” *IEEE transactions on Robotics and Automation*, vol. 13, no. 6, pp. 915–920, 1997.
- [26] G. Van Den Bergen, *Collision detection in interactive 3D environments*. CRC Press, 2003.
- [27] G. Snethen, “Complex collision made simple,” pp. 165–178, 2008.
- [28] J. Pan, S. Chitta, and D. Manocha, “Fcl: A general purpose library for collision and proximity queries,” in *2012 IEEE International Conference on Robotics and Automation*. IEEE, 2012, pp. 3859–3866.
- [29] M. Macklin, “Simulation for learning and robotics: Numerical methods for contact, deformation, and identification,” Ph.D. dissertation, University of Copenhagen, 2020.
- [30] M. Montanari, N. Petrinic, and E. Barbieri, “Improving the gjk algorithm for faster and more reliable distance queries between convex objects,” *ACM Transactions on Graphics (TOG)*, vol. 36, no. 3, pp. 1–17, 2017.
- [31] J. Canny, “Collision detection for moving polyhedra,” *IEEE Transactions on Pattern Analysis and Machine Intelligence*, no. 2, pp. 200–209, 1986.
- [32] X. Qin and N. T. An, “Smoothing algorithms for computing the projection onto a minkowski sum of convex sets,” *Computational Optimization and Applications*, vol. 74, no. 3, pp. 821–850, 2019.
- [33] E. G. Gilbert, “An iterative procedure for computing the minimum of a quadratic form on a convex set,” *SIAM Journal on Control*, vol. 4, no. 1, pp. 61–80, 1966.
- [34] P. Wolfe, “Finding the nearest point in a polytope,” *Mathematical Programming*, vol. 11, pp. 128–149, 1976.
- [35] A. d’Aspremont, D. Scieur, A. Taylor *et al.*, “Acceleration methods,” *Foundations and Trends® in Optimization*, vol. 5, no. 1-2, pp. 1–245, 2021.
- [36] D. Garber and E. Hazan, “Playing non-linear games with linear oracles,” in *2013 IEEE 54th annual symposium on foundations of computer science*. IEEE, 2013, pp. 420–428.
- [37] J. Guélat and P. Marcotte, “Some comments on wolfe’s ‘away step,’” *Mathematical Programming*, vol. 35, no. 1, pp. 110–119, 1986.
- [38] M. Jaggi, “Revisiting frank-wolfe: Projection-free sparse convex optimization,” in *International conference on machine learning*. PMLR, 2013, pp. 427–435.
- [39] T. Kerdreux, A. d’Aspremont, and S. Pokutta, “Projection-free optimization on uniformly convex sets,” in *International Conference on Artificial Intelligence and Statistics*. PMLR, 2021, pp. 19–27.
- [40] S. Lacoste-Julien and M. Jaggi, “On the global linear convergence of frank-wolfe optimization variants,” *Advances in neural information processing systems*, vol. 28, 2015.
- [41] Y. E. Nesterov, “A method of solving a convex programming problem with convergence rate $O(1/k^2)$,” in *Doklady Akademii Nauk*, vol. 269, no. 3. Russian Academy of Sciences, 1983, pp. 543–547.
- [42] J. Nocedal and S. J. Wright, *Numerical optimization*. Springer, 1999.
- [43] F. Bach *et al.*, “Learning with submodular functions: A convex optimization perspective,” *Foundations and Trends® in Machine Learning*, vol. 6, no. 2-3, pp. 145–373, 2013.
- [44] S. Boyd and L. Vandenberghe, *Convex Optimization*. Cambridge University Press, 2004.
- [45] C. A. Holloway, “An extension of the frank and wolfe method of feasible directions,” *Mathematical Programming*, vol. 6, pp. 14–27, 1974.
- [46] T. Kerdreux, A. d’Aspremont, and S. Pokutta, “Restarting frank-wolfe,” in *The 22nd international conference on artificial intelligence and statistics*. PMLR, 2019, pp. 1275–1283.
- [47] G. Dantzig, *Linear programming and extensions*. Princeton university press, 2016.

- [48] C. Carathéodory, “Über den variabilitätsbereich der koeffizienten von potenzreihen, die gegebene werte nicht annehmen,” *Mathematische Annalen*, vol. 64, no. 1, pp. 95–115, 1907.
- [49] B. T. Polyak, “Some methods of speeding up the convergence of iteration methods,” *Ussr computational mathematics and mathematical physics*, vol. 4, no. 5, pp. 1–17, 1964.
- [50] A. Bambade, S. El-Kazdadi, A. Taylor, and J. Carpentier, “Prox-qp: Yet another quadratic programming solver for robotics and beyond,” in *RSS 2022-Robotics: Science and Systems*, 2022.
- [51] J. Pan, S. Chitta, D. Manocha, F. Lamiriaux, J. Mirabel, J. Carpentier *et al.*, “Hpp-fcl: an extension of the flexible collision library,” <https://github.com/humanoid-path-planner/hpp-fcl>, 2015–2022.
- [52] B. Calli, A. Singh, A. Walsman, S. Srinivasa, P. Abbeel, and A. M. Dollar, “The ycb object and model set: Towards common benchmarks for manipulation research,” in *2015 international conference on advanced robotics (ICAR)*. IEEE, 2015, pp. 510–517.
- [53] B. Stellato, G. Banjac, P. Goulart, A. Bemporad, and S. Boyd, “Osqp: An operator splitting solver for quadratic programs,” *Mathematical Programming Computation*, vol. 12, no. 4, pp. 637–672, 2020.
- [54] D. Goldfarb and A. Idnani, “A numerically stable dual method for solving strictly convex quadratic programs,” *Mathematical programming*, vol. 27, no. 1, pp. 1–33, 1983.
- [55] A. Wächter and L. T. Biegler, “On the implementation of an interior-point filter line-search algorithm for large-scale nonlinear programming,” *Mathematical programming*, vol. 106, pp. 25–57, 2006.
- [56] K. Tracy, T. A. Howell, and Z. Manchester, “Differentiable collision detection for a set of convex primitives,” 2022.
- [57] B. Brogliato, A. Ten Dam, L. Paoli, F. Génot, and M. Abadie, “Numerical simulation of finite dimensional multibody nonsmooth mechanical systems,” *Appl. Mech. Rev.*, vol. 55, no. 2, pp. 107–150, 2002.
- [58] Q. L. Lidec, W. Jallet, L. Montaut, I. Laptev, C. Schmid, and J. Carpentier, “Contact models in robotics: a comparative analysis,”
- [59] I. Akkaya, M. Andrychowicz, M. Chociej, M. Litwin, B. McGrew, A. Petron, A. Paino, M. Plappert, G. Powell, R. Ribas *et al.*, “Solving rubik’s cube with a robot hand,” *arXiv preprint arXiv:1910.07113*, 2019.
- [60] J. Carpentier, G. Saurel, G. Buondonno, J. Mirabel, F. Lamiriaux, O. Stasse, and N. Mansard, “The pinocchio c++ library: A fast and flexible implementation of rigid body dynamics algorithms and their analytical derivatives,” in *2019 IEEE/SICE International Symposium on System Integration (SII)*. IEEE, 2019, pp. 614–619.
- [61] C. Mastalli, R. Budhiraja, W. Merkt, G. Saurel, B. Hammoud, M. Naveau, J. Carpentier, L. Righetti, S. Vijayakumar, and N. Mansard, “Crocodyl: An efficient and versatile framework for multi-contact optimal control,” in *2020 IEEE International Conference on Robotics and Automation (ICRA)*. IEEE, 2020, pp. 2536–2542.
- [62] F. Farshidian *et al.*, “Optimal control for switched systems,” <https://github.com/leggedrobotics/ocs2>, 2018.
- [63] L. Montaut, Q. L. Lidec, A. Bambade, V. Petrik, J. Sivic, and J. Carpentier, “Differentiable collision detection: a randomized smoothing approach,” in *2023 IEEE International Conference on Robotics and Automation (ICRA)*, 2022.
- [64] K. Werling, D. Omens, J. Lee, I. Exarchos, and C. K. Liu, “Fast and feature-complete differentiable physics engine for articulated rigid bodies with contact constraints,” in *Robotics: Science and Systems*, 2021.
- [65] Q. Le Lidec, I. Laptev, C. Schmid, and J. Carpentier, “Differentiable rendering with perturbed optimizers,” *Advances in Neural Information Processing Systems*, vol. 34, pp. 20 398–20 409, 2021.
- [66] R. Budhiraja, J. Carpentier, C. Mastalli, and N. Mansard, “Differential dynamic programming for multi-phase rigid contact dynamics,” in *2018 IEEE-RAS 18th International Conference on Humanoid Robots (Humanoids)*. IEEE, 2018, pp. 1–9.
- [67] W. Jallet, A. Bambade, N. Mansard, and J. Carpentier, “Constrained differential dynamic programming: A primal-dual augmented lagrangian approach,” in *2022 IEEE/RSJ International Conference on Intelligent Robots and Systems (IROS)*. IEEE, 2022, pp. 13 371–13 378.

BIOGRAPHY



Louis Montaut received an M.Sc. degree in Mathematics, Computer Vision and Machine Learning from École des Ponts et Chaussées in Paris. Since 2020, he is a Ph.D. student in the Willow team at Inria, École Normale Supérieure de Paris and FEL CVUT in Prague. He is one of the main developers of HPP-FCL.



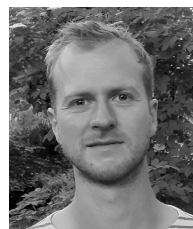
Quentin Le Lidec is a Ph.D. student in the Willow team at Inria and École Normale Supérieure. Prior to that, he received an engineering degree from Ecole Polytechnique and an M.Sc. degree in Mathematics, Computer Vision, and Machine Learning from École Normale Supérieure Paris-Saclay.



Vladimir Petrik received the M.Sc. degree in cybernetics and robotics and the Ph.D. degree in artificial intelligence and biocybernetics from the Czech Technical University in Prague, Czech Republic, in 2014 and 2019, respectively. From 2018 to 2019, he was a Visiting Researcher at Aalto University, Finland, after which he spent four months within the Willow research group at Inria in France. Since 2019, he has been a Researcher at the Czech Institute of Informatics, Robotics and Cybernetics, Czech Technical University in Prague.



Josef Sivic holds a distinguished researcher position at the Czech Institute of Robotics, Informatics and Cybernetics at the Czech Technical University in Prague where he heads the Intelligent Machine Perception team and the ELLIS Unit Prague. He received the habilitation degree from École Normale Supérieure in Paris in 2014 and PhD from the University of Oxford in 2006. After Phd he was a post-doctoral associate at the Computer Science and Artificial Intelligence Laboratory at the Massachusetts Institute of Technology. He received the British Machine Vision Association Sullivan Thesis Prize, three test-of-time awards at major computer vision conferences, an ERC Starting Grant, and an ERC Advanced Grant.



Justin Carpentier is a researcher at Inria and École Normale Supérieure, leading the Willow research team since 2023. He graduated from École Normale Supérieure Paris-Saclay in 2014 and received a Ph.D. in Robotics in 2017 from the University of Toulouse. He did his Ph.D. in the Gepetto team at LAAS-CNRS in Toulouse, working on the computational foundations of legged locomotion. His research interests lie at the interface of optimization, machine learning, computer vision, and control for robotics, with applications ranging from agile locomotion to dexterous manipulation. He is also the main developer and manager of widely used open-source robotics software, among them Pinocchio, Prox-Suite, HPP-FCL, and Aligator.